# Politecnico di Milano

# Reduced models in cardiac electrophysiology

## Applications to the inverse problem

Candidato:
**Elisa SCHENONE**
Matricola 739281

Relatore:
**Prof. Luca FORMAGGIA**

Correlatori:
**Prof. Jean-Frédéric GERBEAU**
**Prof.ssa Muriel BOULAKIA**

*"Abbiamo tutti problemi di cuore..."*
Sv.

**Abstract**

This Master Thesis is the result of a six month internship in the REO group of the *Insitut Nationale de Recherche Informatique et Automatique* (INRIA) of Rocquencourt - Paris (France), under the supervision of Jean-Frédéric Gerbeau and Muriel Boulakia. This work aim is the application of the Proper Orthogonal Decomposition (POD) as a reduced model technique in cardiac electrophysiology. The main features used to solve and treat this problem are the bi-domain model, the Mitchell and Schaeffer ionic model and the *Electrocardiogram* (ECG). Particularly, we focused on two medical studies: myocardial transmural infarction and accelerated beats. In both cases we numerically solved the problem with a complete model and with a reduced one and we faced with an inverse problem. In the study of the myocardial infarction we are aimed to find the infarcted area starting from a simulated ECG, applying a *genetic algorithm*. In the case of the simulation of a long sequence of accelerated beats, the solutions and the corresponding ECG are used to build the so-called *restitution curve*. Once obtained the restitution curve, i.e. a relationship between the two main phases of a cardiac beat, we applied some theoretical results in order to estimate some parameters of the ionic model. Dealing with this last part, here is presented a preliminary study useful for future work.

## Acknowledgements

Innanzitutto ringrazio il professor Luca Formaggia per avermi dato la possibilità di partire e per l'entusiasmo con cui mi ha aiutato e consigliato.

Je remercie Jean-Frédéric Gerbeau pour m'avoir accueillie dans son équipe et pour m'avoir donné la chance de travailler avec son groupe. Je remercie aussi Muriel Boulakia pour le temps qu'elle m'a consacré, pour tout ce qu'elle m'a appris et pour la patience qu'elle a eue avec moi.

Merci à l'equipe SISYPHE de Michel Sorine pour avoir traité nos données et pour leur algorithme de détection de fin d'onde T.

Merci à tout le Bâtiment 16, aux chercheurs et aux doctorants (et aussi aux ingénieurs). Pendant ces six mois j'ai appris à travailler dans une équipe, à partager de belles pauses et parfois des moments difficiles. Merci en particulier à Vincent pour son aide avec Ubuntu, à Cesare pour les discussions, les comparaisons et l'aide, et à Saverio.

Un grazie ai miei genitori per avermi dato la possibilità di studiare, mi hanno sempre invogliato ad andare avanti, mi hanno supportato in ogni mia scelta e continuano a farlo.

Infine, non ci sarebbe stata la tesi a Parigi senza cinque anni di Poli. Grazie ai miei compagni di studi (e non solo) per aver condiviso questo percorso con me. E grazie all'AIM per avermi fatto conoscere un aspetto nuovo degli ingegneri matematici, per le riunioni e per le discussioni, per i tornei e per gli aperitivi, e soprattutto per gli amici. Non ultimo, grazie a chi mi ha convinto a partire nonostante non fosse la scelta più facile.

# Contents

# Introduction

The first aim of this project is to study some applications of a model reduction method, which is a very important technique used to decrease the computational time of various kinds of problems. The model reduction method that we used is the Proper Orthogonal Decomposition technique, described in chapter 2 and the application domain presented here is the cardiac electrophysiology.

The cardiac electrophysiology is the study of the electrical activity of the heart tissues and the main tool used to measure it is the Electrocardiogram. To simulate the evolution of the heart potential we choose the bidomain model described hereafter. Both the resolutions of the direct problem and of the inverse problem, i.e. the identification of the parameters of the corresponding equations, are very useful. Particularly, we decided to apply our studies to two main applications: the case of an infarction and the study of accelerated beats.

Hereafter we give a brief description of the functioning of the heart and of the procedure of the electrocardiogram. Further details can be found in the doctoral thesis of Néjib Zemzemi [22], which constitutes the starting point of the presented work. We end this introduction with a presentation of the objectives of this work.

## The heart

The heart is a hollow muscle located in the chest between the lungs behind the sternum and above the diaphragm. Its role is to pump the blood to the whole body: most of the human organs cannot survive more than few minutes without supply of oxygenated blood.

The heart is divided into four parts (two atria and two ventricles) and it is mainly composed of oriented fibers. The blood is pumped by the heart thanks to a series of contractions (*systoles*) and relaxations (*diastoles*) of atria and ventricles. The heart contracts regularly, at rest about 70 times a minute and it can reach the 180 beats a minute, or even 210 in case of great efforts. Contractions of the heart are intrinsic: each cardiac cell beats regularly and spontaneously.
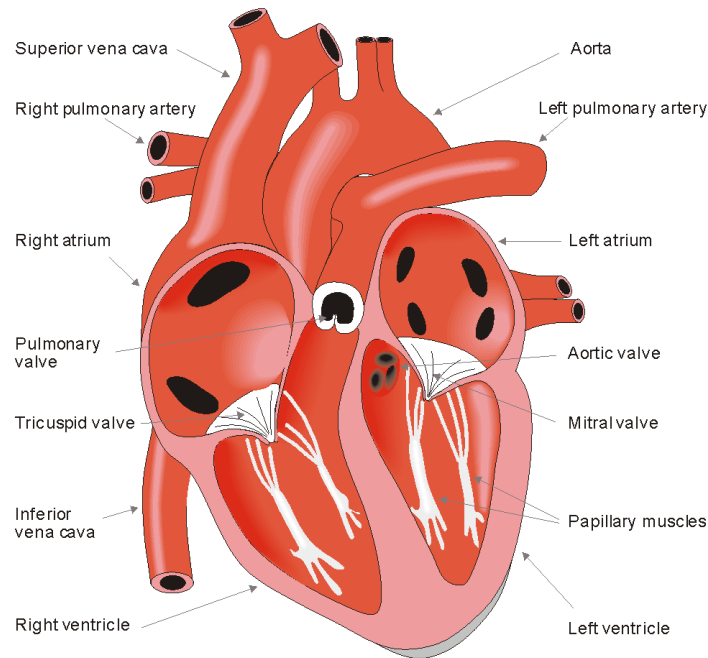
Figure 1: The anatomy of the heart (Source: bembook [10]).

The cardiac beats are controlled by a group of cells, located in the right atrium at the superior vena cava and called sinus node, that are self-excitatory. From the sinus node, activation propagates throughout the atria to the ventricles. Propagation from the atria to the ventricles is provided by a specialized conduction system, composed of a common bundle called the *bundle of His*. This system separates into a left and a right bundle brunches, propagating along each side of the septum, then the bundles ramify into *Purkinje fibers*.

## The electrocardiogram

Electrocardiogram (ECG) is the most used exam providing an interpretation of the heart's electrical activity. In practice, it records by skin electrodes the voltage of different body's points, these measures (or *leads*) are then represented as twelve graphs of the recorded voltage vs time. There are many exams that can be done to study the heart behavior, the ECG is largely used since it is a non invasive and inexpensive one.

The voltage between the body surface's points is measured by the *electrocardiograph*, i.e. the device that allows to do an ECG, and it is printed on a display, called *electrocardioscope*, or on a so-called *graph paper*. Figure 3 shows the first ECG lead in an healthy case. The different waves we can
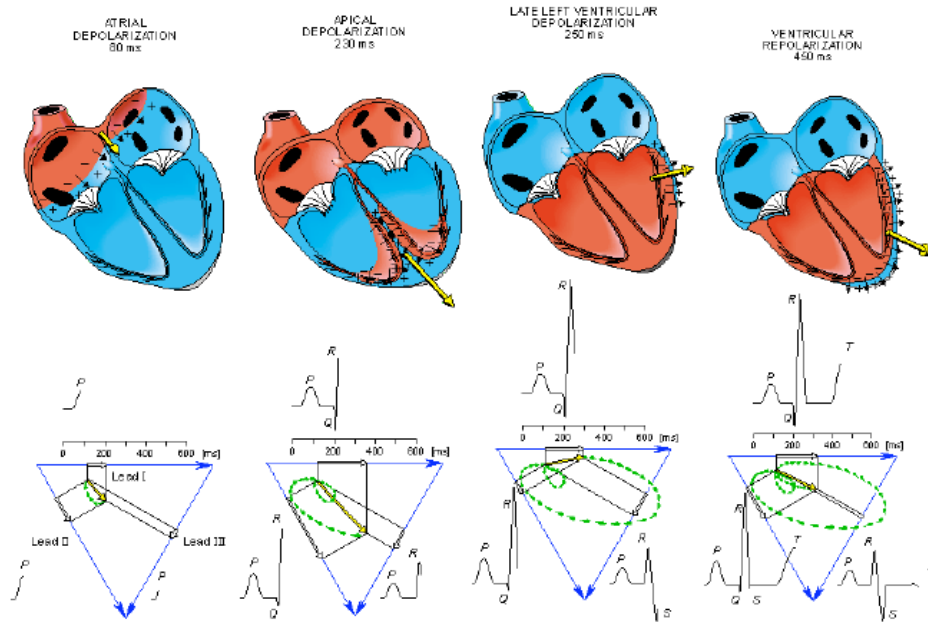
Figure 2: Cardiac mechanical activity steps and corresponding ECG components (Source: bembook [10]).

see are called (from left to right) P, Q, R, S, T and U waves. The P wave represents the auricular depolarization, the QRS complex represents the ventricular depolarization, the segment QT is the plateau of the ventricular action potential, the T wave corresponds to the ventricular re-polarization and the U wave (generally absent) is due to a mechanical factor that corresponds to the myocardium relaxation.

## Objectives

As we want to use the ECG as main tool to analyze our results, we need to describe the evolution of the potential of the hearth during each beat. To study the electrical behavior of the heart we use the so-called *bidomain model*. The biological principles and the mathematical equations that describe this model are exposed in the next chapter.

Once the model is defined, our aim is to apply the POD method. In a first step this method is used for the resolution of the direct problem in the case of a patient suffering of a stroke or infarction. Infarction is a very common pathology: it is due to a lack of blood supply in a zone of the heart which leads to the damage of the tissue. We simulate different kinds of infarctions located in some area of the left ventricle and we verify that
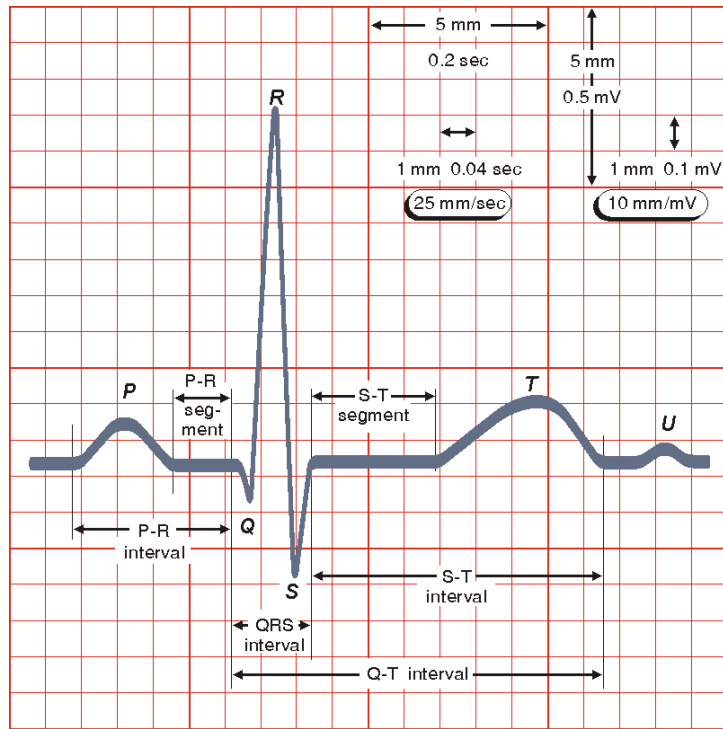
Figure 3: The normal electrocardiogram (Source: bembook [10]).

the corresponding simulated ECG is in accordance with the medical theory. Then, using a well chosen POD basis (for further details see chapter 2) we simulate an infarction located in a random point of the left ventricle.

Once this basis is build, we can use it also to solve the inverse problem. The idea is to use an ECG (real or simulated) to find out some parameters of the model. In the case of the study of infarction our aim is to find the coordinates on the left ventricle surface of the infarcted zone, using a genetic algorithm. Genetic algorithms (described in chapter 3) are a heuristic kind of optimization method based on the subsequent resolution of the function that has to be minimized. The use of the POD allows to reduce significantly the computational time of resolution.

The second application of the POD is the resolution of a long sequence of accelerated beats. This simulation allows to obtain the so-called *restitution curve*, i.e. the dependence between diastolic interval (DI) and the successive duration of a cardiac action potential (APD). This curve is known to be important in the understanding of some arrhythmias ([19], [12]). The simulation of the restitution curve is extremely challenging for 3D models since it requires several dozen of heart beats, whereas the simulation of one heart beat is already very demanding. The study of a restitution curve, by definition, can be conducted on a single cell, recording its transmembrane

potential, or looking at the ECG first lead. In fact, DI and APD can be respectively compared to the TQ time (time between the T and the Q wave) and the QT time ([11]). Once obtained the restitution curve, we used them to find some parameters of the ionic model. In this work we presented only a preliminary study of these tools, future developments will probably lead to more interesting results.

## Contents of the work

In the first part of the work we present the mathematical instruments: first chapter describes the bidomain model and the ionic model, while second and third ones respectively deal with the POD method and the genetic algorithms description.

The second part treats the first application: the simulation of a transmural myocardial infarction. We first face to the numerical simulation of an infarction, then we look for a good POD basis and we use it to solve the inverse problem of identification of the infarcted area.

The third part deals with the study of long sequence of accelerated beats and the restitution curves. First, a preliminary study on the single cell model and the corresponding restitution curve, used to estimate some ionic parameters, is done. Then this results are extended to the 3D model: the numerical solution and the corresponding restitution curve is calculated both with the complete and the reduced models, and a first approach to the identification of ionic parameters is presented.

Finally, some conclusions and future possibility of works are drawn.

# Introduzione

Il principale obiettivo della presente tesi é l'applicazione del metodo di riduzione dei modelli, tecnica di largo utile alla diminuzione dei tempi di calcolare in una vasta categoria di problemi. Il metodo di riduzione dei modelli utilizzato per questo progetto è la Proper Orthogonal Decomposition, descritta nel capitolo 2, ed é stata applicata in particolare al campo dell'elettrofisiologia cardiaca.

L'elettrofisiologia cardiaca è lo studio dell'attività elettrica del cuore e il principale strumento utilizzato per questo studio è l'elettrocardiogramma. Per simulare l'andamento del potenziale elettrico cardiaco abbiamo scelto il cosiddetto modello *bidomain* descritto nel seguito. Sia la risoluzione del problema diretto, sia quella del problema inverso, ovvero l'identificazione dei parametri delle equazioni caratteristiche del modello, sono di largo uso. In particolare, abbiamo deciso di fare riferimento a due casi di interesse medico: la simulazione di un infarto del miocardio e lo studio di battiti accelerati.

Di seguito, una breve descrizione del funzionamento del cuore e della procedura per ottenere un elettrocardiogramma. Maggiori dettagli possono essere trovati nella tesi di dottorato di Néjib Zemzemi [22], che costituisce il punto di partenza del presente lavoro. Concludiamo questa introduzione con una presentazione degli obiettivi del lavoro.

## Il cuore

Il cuore è un muscolo cavo collocato nella cassa toracica tra le costole e lo sterno, al di sopra del diaframma. Il suo ruolo è quello di pompare il sangue nell'intero corpo: la maggior parte degli organi umani non può sopravvivere più di qualche minuto senza apporto di sangue ossigenato.

Il cuore è diviso in quattro parti (due atri e due ventricoli) ed è principalmente composto da fibre orientate. Il sangue è pompato dal cuore grazie ad una serie di contrazioni (*sistole*) e di rilassamenti (*diastole*) di atri e ventricoli. Il cuore si contrae regolarmente, a riposo circa 70 volte al minuto e può raggiungere i 180 battiti al minuto, o anche i 210 in caso di grande sforzo. Le contrazioni del cuore sono intrinseche: ogni cellula cardiaca batte regolarmente in modo spontaneo.

I battiti cardiaci sono controllati da un gruppo di cellule, chiamate nodo sinusale, collocate nell'atrio destro, nella vena cava superiore, e che sono auto-eccitanti. Dal nodo sinusale, l'attivazione si propaga attraverso gli atri e i ventricoli. La propagazione dagli atri ai ventricoli è garantita da un sistema di conduzione specializzato, composto da un fascio comune chiamato *fascio di His*. Questo sistema si separa in una branca destra ed in una branca sinistra, che si propagano lungo i due lati del setto, successivamente i fasci si ramificano nelle *fibre di Purkinje*.

## L'elettrocardiogramma

L'elettrocardiogramma (ECG) è l'esame più usato per avere un'interpretazione dell'attività elettrica del cuore. In pratica, la differenza di potenziale in diversi punti del corpo viene registrata tramite elettrodi cutanei, queste misure (dette *derivazioni*) sono quindi rappresentate come dodici grafici della differenza di potenziale in funzione del tempo. Ci sono molti esami che possono essere usati per lo studio del comportamento cardiaco, l'ECG è largamente diffuso in quanto risulta non invasivo e poco costoso.

La differenza di potenziale tra i punti della superficie del corpo è misurata dall'*elettrocardiografo*, ovvero una macchina che permette di calcolare un ECG, ed è stampato su un display, chiamato *elettrocardioscopo*, o sulla cosiddetta *carta millimetrata*. La Figura 3 mostra la prima derivazione dell'ECG in un caso sano. Le diverse onde che si possono vedere sono chiamate (da sinistra verso destra) onde P, Q, R, S, T e U. L'onda P rappresenta la depolarizzazione auricolare, il complesso QRS rappresenta la depolarizzazione ventricolare, il segmento QT è il plateau del potenziale d'azione ventricolare, l'onda T corrisponde alla repolarizzazione ventricolare e l'onda U (generalmente assente) è dovuta a un fattore meccanico corrispondente al rilassamento del miocardio.

## Obiettivi

Poichè abbiamo usato l'ECG come strumento principale di misura dei risultati, abbiamo bisogno di descrivere il potenziale elettrico del cuore durante ogni singolo battito. Per studiare il comportamento elettrico del cuore usiamo il cosiddetto modello *bi-dominio*. Il principio biologico e le equazioni matematiche che descrivono questo modello sono riportati nel capitolo successivo.

Definito il modello, il nostro obiettivo è di applicare il metodo di riduzione del modello in analisi: la *Proper Orthogonal Decomposition* (POD). La prima applicazione riguarda la risoluzione numerica del problema, ovvero delle equazioni che descrivono il potenziale cardiaco in grado di simulare l'ECG di un paziente colpito da ictus o infarto. L'infarto è una patologia

molto comune: si tratta di un mancato apporto di flusso sanguigno in una zona del cuore che può causare complicazioni e morte. Il nostro obiettivo è di simulare diversi tipi di infarto, in particolare di tipo transmurale, posizionati in alcune zone del ventricolo sinistro. Risolto il sistema di equazioni, verifichiamo che il corrispondente ECG sia in accordo con la teoria medica. Quindi, usando una base POD scelta in modo opportuno (per maggiori dettagli riferirsi al capitolo 2), simuliamo un infarto posizionato in un qualunque punto del ventricolo sinistro.

Una volta trovata la base adatta, essa può essere usata anche per la risoluzione del problema inverso. L'idea è di utilizzare un ECG (reale o simulato) per trovare alcuni parametri del modello. Nel caso dello studio di un infarto il nostro obiettivo è trovare le coordinate sulla superficie del ventricolo sinistro corrispondenti alla zona colpita, usando delgli algoritmi genetici. Gli algoritmi genetici (descritti nel capitolo 3) sono metodi di ottimizzazione euristici basati sulla ripetuta risoluzione della funzione che si vuole minimizzare, da cui l'importanza di usare la POD per ridurre il tempo computazionale di risoluzione.

La seconda applicazione nella quale è stata utilizzata la tecnica della POD è la simulazione di una lunga sequenza di battiti. È di particolare interesse lo studio della cosiddetta *curva di restituzione*, ovvero la dipendenza tra l'intervallo diastolico (DI) e la successiva durata del potenziale d'azione (Action Potential Duration - APD). Questa curva è importante per capire alcuni tipi di aritmia cardiaca ([19], [12]). La ricostruzione della curva di restituzione è estremamente costosa per un modello 3D poichè richiede la simulazione di decine di battiti cardiaci. Ricordiamo che la simulazione di un solo battito è già computazionalmente molto onerosa. Lo studio della curva di restituzione, per la definizione di APD, può essere condotto su una singola cellula, misurando il suo potenziale d'azione, oppure osservando la prima derivazione di un ECG. Infatti, DI e APD possono essere comparati rispettivamente con il tempo TQ (tempo trascorso tra l'onda T e l'onda Q) e il tempo QT ([11]). Una volta ottenuta la curva di restituzione, essa viene usata per trovare alcuni dei parametri del modello ionico. In questo lavoro viene presentato uno studio preliminare di questi strumenti, sviluppi futuri porteranno probabilmente a migliori risultati.

## Piano del lavoro

Nella prima parte del lavoro vengono presentati gli strumenti matematici utilizzati: il primo capitolo descrive il modello bi-dominio ed il modello ionico, mentre nel secondo e nel terzo vengono rispettivamente decritti il metodo della POD e gli algoritmi genetici.

La seconda parte del lavoro è inccentrata sullo studio di un'applicazione medica: la simulazione di un infarto transmurale del miocardio. Abbiamo

prima affrontato la simulazione numerica di un infarto, cercato una base POD adatta ad approssimare il problema e l'abbiamo utilizzata per risolvere il problema inverso di identificazione dell'area malata.

La terza parte si occupa dello studio di lunghe sequenze di battiti accelerati e delle curve di restituzione. Innanzitutto, viene presentato uno studio preliminare condotto sul modello di una singola cellula e sulla curva di restituzione corrispondente. Quest'ultima viene poi utilizzata per stimare alcuni parametri ionici. Successivamente i risultati ottenuti sul sistema 0D vengono estesi al sistema 3D: le soluzioni numeriche e le corrispondenti curve di restituzione vengono calcolate sia con il modello completo che con quello ridotto, e viene presentato un primo approccio all'identificazione dei parametri ionici.

Infine, vengono esposte le principali conlcusioni e i possibili sviluppi del lavoro.

# Part I

# Modeling of the electrical activity of the heart

# Chapter 1

# Mathematical models

In this first chapter, we introduce the mathematical model used in this work to describe the behavior of the electrical activity of the heart. In the last section 1.4, we briefly present the numerical methods and the results obtained in [2] and [22].

## 1.1 Heart model

Here we use the so-called bidomain model to describe the electrical behavior of the heart. This model is based on the assumption that at microscopic scale the cardiac tissue is composed of two different domains: the intra and the extra-cellular ones. To better understand the model, we first present what occurs at the cellular scale and we then present the model at the macroscopic scale.

### 1.1.1 Microscopic scale

Each cell is surrounded by a membrane, this membrane is uncovered of proteins whose role is to assure the flux of different substances from intra to extra-cellular zones, and viceversa. These proteins can have a passive or an active behavior, and the exchange of certain chemical substances causes the cellular depolarization and repolarization. We can classify this ionic transport into three types: ionic channels, pumps and exchangers.

A ionic channel allows a chemical substance to pass through the cellular membrane in the direction of electrochemical gradient. It doesn't need any energy contribution of the cell. Then this kind of transport is called passive. The cell's depolarization is caused by the opening of ionic channel corresponding to the sodium $Na^+$. The opening of this channel causes the creation of a ionic current $I_{Na^+}$ (of the order of a pico-ampére).

On the contrary to ionic channels, pumps allow substances to get through the membrane in the opposite direction. This exchange obviously needs the
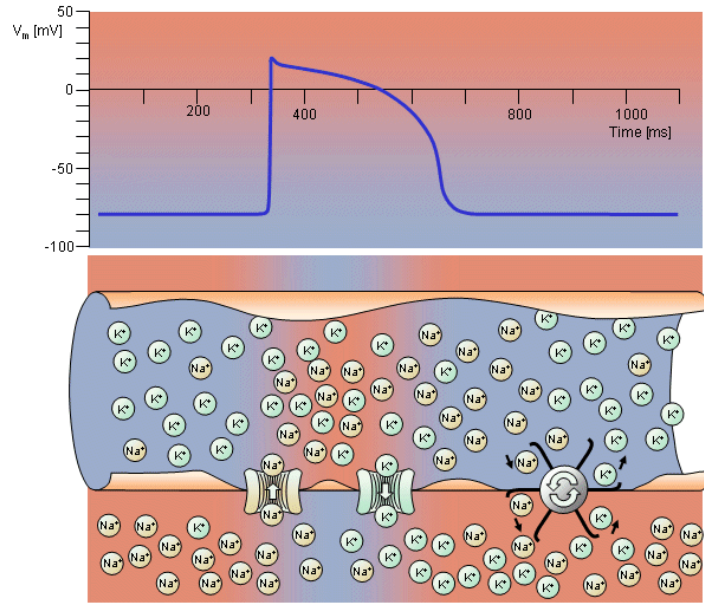
Figure 1.1: Electrophysiology of the cardiac muscle cell (Source: bembook [10]). Ionic channels and pumps are represented for the transports of $Na^+$ and $K^+$.

work of some proteins: the Adenosine Tri Phosphate molecules (ATP).

The most important pump is the one that allows sodium/potassium ($Na/K$) exchanges. This pump lets two potassium ions $K^+$ enter into the cell while three sodium ions $Na^+$ get out. At rest, the cell is strongly concentrated in potassium and weakly concentrated in sodium, during depolarization phase the ionic channels let the sodium sin and let the potassium out. Once the cell is depolarized, it is enriched in sodium and poor in potassium, the activation of $Na/K$ pump allows the cell to find its natural concentrations back. When activated, the $Na/K$ pump creates a ionic current $I_{Na/K}$.

Finally, the exchangers transport ions between the intra and extra-cellular domain. The ions are exchanged using the electrochemical gradient energy of another kind of ions. For instance, we can consider the $Na^+/Ca^{2+}$ exchanger: it uses the energy of the $Na/K$ pump to transport $Na^+$ and $Ca^{2+}$ and allows the concentrations of these substances to find the equilibrium again.

To sum up, each cell polarization cycle can be divided into four parts.

- At rest the cell is strongly concentrated in $K^+$, and the transmembrane potential $V_m$ (the difference in potential between the intra and the extra-cellular domain potentials) is negative.

- In the first phase the $Na$ ionic channel opens and lets ions $Na^+$ enter

into the cell, so we finally have a higher concentration of $Na^+$; this movement creates a negative current $I_{Na^+}$ and the transmembrane potential increases.

- Then there is a phase of *plateau*, the $Ca/Na$ exchanger lets ions $Ca^{2+}$ in and lets ions $Na^+$ out, in this phase the total ionic current is negligible and $V_m$ is almost constant.

- During the third phase the action of the $Na/K$ pump induces the increasing of the $K^+$ concentration in the cell and creates a current positive $I_{Na/K}$, consequently the transmembrane potential $V_m$ increases.

- Finally, the $Na^+/Ca^{2+}$ exchanger brings back the concentrations to the equilibrium: ions $Na^+$ come into the cell and ions $Ca^{2+}$ go out, while the ionic current in this phase is negligible and $V_m$ is almost constant.

The intra-cellular domain is composed of cardiac muscle cells, while the extra-cellular domain is composed of the rest of the media. We denote $\Omega_{\mathrm{H}}$ the total domain occupied by the heart, and $\Omega_{\mathrm{H_i}}$, $\Omega_{\mathrm{H_e}}$ the intra and the extra-cellular subdomains: $\overline{\Omega_{\mathrm{H}}} = \overline{\Omega_{\mathrm{H_i}}} \cup \overline{\Omega_{\mathrm{H_e}}}$.

We denote by $\mathbf{j}_i$, $\mathbf{j}_e$, $u_i$, $u_e$ and $\boldsymbol{\sigma}_i$, $\boldsymbol{\sigma}_e$, respectively, the current density, the electric potential and the conductivity of the intra and the extra-cellular domains. Thanks to Ohm's law we can write:

$$\mathbf{j}_i = -\boldsymbol{\sigma}_i \boldsymbol{\nabla} u_i,$$
$$\mathbf{j}_e = -\boldsymbol{\sigma}_e \boldsymbol{\nabla} u_e.$$

The intra and the extra-cellular domains are separated by a membrane $\Gamma_{\mathrm{m}} = \partial\Omega_{\mathrm{H_i}} \cap \partial\Omega_{\mathrm{H_e}}$. Applying the conservation of the charge on $\Gamma_{\mathrm{m}}$ we obtain

$$I_{\mathrm{m}} = \mathbf{j}_i \cdot \mathbf{n} = -\mathbf{j}_e \cdot \mathbf{n}, \tag{1.1}$$

where $I_{\mathrm{m}}$ is the surface current density on $\Gamma_{\mathrm{m}}$ and $\mathbf{n}$ is the outer unit normal vector of $\partial\Omega_{\mathrm{H_i}}$. The ionic exchanges are described by a ionic current $I_{\mathrm{ion}}$, so we can write the surface current density as

$$I_{\mathrm{m}} = I_{\mathrm{ion}} + C_{\mathrm{m}}\frac{\partial V_{\mathrm{m}}}{\partial t} + i_{\mathrm{app}}, \tag{1.2}$$

where $C_{\mathrm{m}}$ is the membrane capacity (per surface unit), $V_{\mathrm{m}}$ is the transmembrane potential:

$$V_{\mathrm{m}} = u_i - u_e,$$

and $i_{\mathrm{app}}$ is the applied current (we can say from an external source). $I_{\mathrm{ion}}$ depends on $V_{\mathrm{m}}$ and on a variable field $\mathbf{w}$, which represents different chemical

concentrations and some variables on which the opening and closing of ionic channels gates depend: $I_{\text{ion}} = I_{\text{ion}}(V_{\text{m}}, \mathbf{w})$. In general we can write

$$\frac{\partial \mathbf{w}}{\partial t} + \mathbf{g}(V_{\text{m}}, \mathbf{w}) = 0,$$

where $\mathbf{g}$ is a function which will be described by a model representing the ionic exchanges through the cellular membrane. In this paper we have considered the Mitchell and Schaeffer model (see section 1.3).

### 1.1.2 Macroscopic scale

Equation (1.2) represents a discrete description of the model on the different domains $\Omega_{\text{H}_\text{i}}$, $\Omega_{\text{H}_\text{e}}$. Doing an homogenization process we can find a model, continuous on the global domain $\Omega_{\text{H}}$, in which each variable is replaced by its mean value. So we can write (1.1) as

$$\text{div}(\boldsymbol{\sigma}_{\text{i}} \boldsymbol{\nabla} u_{\text{i}} + \boldsymbol{\sigma}_{\text{e}} \boldsymbol{\nabla} u_{\text{e}}) = 0, \text{ on } \Omega_{\text{H}},$$

or, since $V_{\text{m}} = u_{\text{i}} - u_{\text{e}}$,

$$\text{div}((\boldsymbol{\sigma}_{\text{i}} + \boldsymbol{\sigma}_{\text{e}}) \boldsymbol{\nabla} u_{\text{e}}) = -\text{div}(\boldsymbol{\sigma}_{\text{i}} \boldsymbol{\nabla} V_{\text{m}}), \text{ on } \Omega_{\text{H}}. \tag{1.3}$$

From (1.2) we can find the homogenized equation

$$A_{\text{m}}\big(C_{\text{m}}\frac{\partial V_{\text{m}}}{\partial t} + I_{\text{ion}}(V_{\text{m}}, \mathbf{w})\big) - \text{div}(\boldsymbol{\sigma}_{\text{i}} \boldsymbol{\nabla} V_{\text{m}}) = \text{div}(\boldsymbol{\sigma}_{\text{i}} \boldsymbol{\nabla} u_{\text{e}}) + I_{\text{app}}, \text{ on } \Omega_{\text{H}}, \tag{1.4}$$

where $A_{\text{m}}$ is a geometric constant which represents the average rate of surface membrane per volume unit and $I_{\text{app}}$ is the applied current.

We still need boundary conditions to close the equations system. The boundary of the heart is divided into two different zones: the endocardium (that we denote $\Gamma_{\text{endo}}$), which is the internal membrane, and the epicardium ($\Gamma_{\text{epi}}$), the external one. We just have to impose that on the surface of the heart $\Sigma = \Gamma_{\text{endo}} \cup \Gamma_{\text{epi}}$ the intra-cellular current $\mathbf{j}_{\text{i}}$ does not propagate outside the heart:

$$\boldsymbol{\sigma}_{\text{i}} \boldsymbol{\nabla} u_{\text{i}} \cdot \mathbf{n} = 0, \text{ on } \Sigma,$$

where $\mathbf{n}$ is the outer unit normal vector of $\Sigma$. In terms of $V_{\text{m}}$ and $u_{\text{e}}$:

$$\boldsymbol{\sigma}_{\text{i}} \boldsymbol{\nabla} u_{\text{e}} \cdot \mathbf{n} = -\boldsymbol{\sigma}_{\text{i}} \boldsymbol{\nabla} V_{\text{m}} \cdot \mathbf{n}, \text{ on } \Sigma. \tag{1.5}$$

Finally, if we consider an uncoupled heart-thorax model, we can impose that the heart is isolated from the outside:

$$\boldsymbol{\sigma}_{\text{e}} \boldsymbol{\nabla} u_{\text{e}} \cdot \mathbf{n} = 0, \text{ on } \Sigma. \tag{1.6}$$

We obtain the isolated bidomain model:

$$
\begin{aligned}
A_{\mathrm{m}}\left(C_{\mathrm{m}}\tfrac{\partial V_{\mathrm{m}}}{\partial t} + I_{\mathrm{ion}}(V_{\mathrm{m}}, \mathbf{w})\right) - \mathrm{div}(\boldsymbol{\sigma}_{\mathrm{i}}\boldsymbol{\nabla}V_{\mathrm{m}}) &= \mathrm{div}(\boldsymbol{\sigma}_{\mathrm{i}}\boldsymbol{\nabla}u_{\mathrm{e}}) + I_{\mathrm{app}}, & \Omega_{\mathrm{H}} \\
\mathrm{div}((\boldsymbol{\sigma}_{\mathrm{i}} + \boldsymbol{\sigma}_{\mathrm{e}})\boldsymbol{\nabla}u_{\mathrm{e}}) &= -\mathrm{div}(\boldsymbol{\sigma}_{\mathrm{i}}\boldsymbol{\nabla}V_{\mathrm{m}}), & \Omega_{\mathrm{H}} \\
\partial_t\mathbf{w} + \mathbf{g}(V_{\mathrm{m}}, \mathbf{w}) &= 0, & \Omega_{\mathrm{H}} \\
\boldsymbol{\sigma}_{\mathrm{i}}\boldsymbol{\nabla}V_{\mathrm{m}} \cdot \mathbf{n} &= -\boldsymbol{\sigma}_{\mathrm{i}}\boldsymbol{\nabla}u_{\mathrm{e}} \cdot \mathbf{n}, & \Sigma \\
(\boldsymbol{\sigma}_{\mathrm{i}} + \boldsymbol{\sigma}_{\mathrm{e}})\boldsymbol{\nabla}u_{\mathrm{e}} \cdot \mathbf{n} &= -\boldsymbol{\sigma}_{\mathrm{i}}\boldsymbol{\nabla}V_{\mathrm{m}} \cdot \mathbf{n}, & \Sigma.
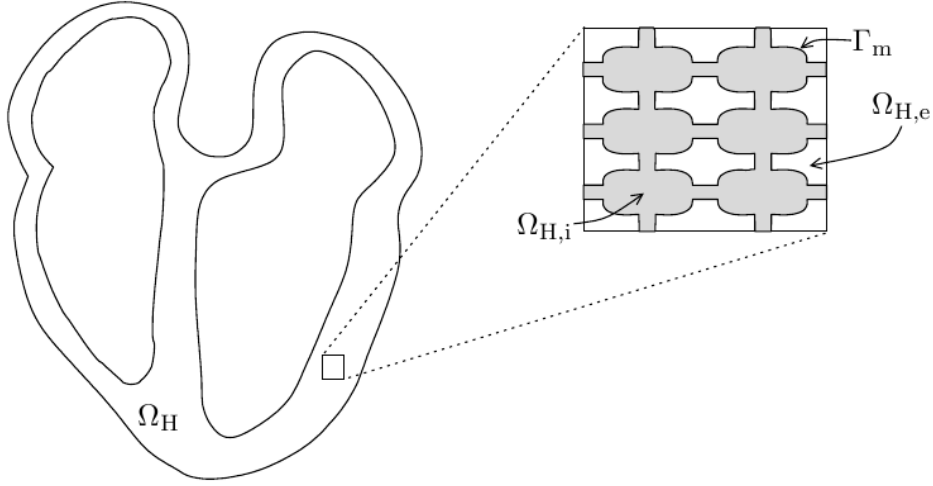\end{aligned}
\tag{1.7}
$$



Figure 1.2: Heart cut with bidomain model (Source: [22]).

## 1.2 Thorax model and coupling

To simulate an electrocardiogram we need to evaluate the voltage in some thorax points, so we want to write a model for the thorax and to couple it with the heart's one.

We denote $\Omega_{\mathrm{T}}$ and $u_{\mathrm{T}}$ the domain and the electric potential of the thorax and we consider it as a passive conductor, so we just have to solve a Poisson equation. If we denote $\mathbf{j}_T$ the volume current density of the thorax, applying Ohm's law, we find

$$
\mathbf{j}_{\mathrm{T}} = -\boldsymbol{\sigma}_{\mathrm{T}}\boldsymbol{\nabla}u_{\mathrm{T}}, \ \text{on } \Omega_{\mathrm{T}},
$$

where, as usual, $\boldsymbol{\sigma}_{\mathrm{T}}$ represents the thorax conductivity tensor. The conservation of the charge can be simply written as

$$
\mathrm{div}(\boldsymbol{\sigma}_{\mathrm{T}}\boldsymbol{\nabla}u_{\mathrm{T}}) = 0, \ \text{on } \Omega_{\mathrm{T}}.
\tag{1.8}
$$

The boundary conditions to impose are the non conductivity outside the external domain $\Gamma_{\mathrm{ext}}$:

$$
\boldsymbol{\sigma}_{\mathrm{T}}\boldsymbol{\nabla}u_{\mathrm{T}} \cdot \mathbf{n}_T = 0, \ \text{on } \Gamma_{\mathrm{ext}},
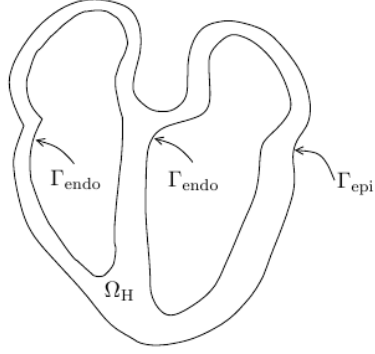$$

Figure 1.3: Heart cut with epicardium and endocardium (Source: [22]).



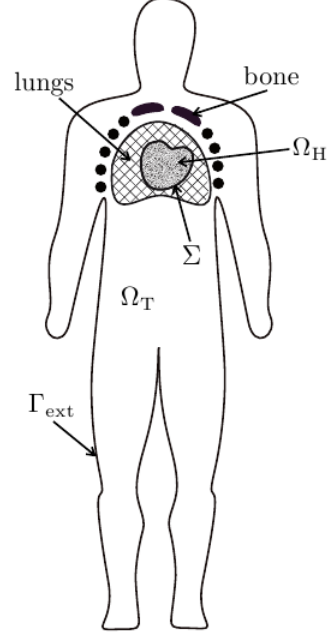Figure 1.4: Cardiac domain and thorax domain (Source: [22]).

with $\mathbf{n}_T$ the outer unit normal vector of $\Gamma_{\text{ext}}$, and a coupling condition with the heart on $\partial\Omega_T \setminus \Gamma_{\text{ext}} = \Sigma$.

To complete our coupled model we have to impose some transmission conditions of potential and current from $\Omega_H$ to $\Omega_T$. So, we suppose on $\Sigma$ the potential and current continuity between the extra-cellular values and the thorax ones. These conditions can be reduced to:

$$
\begin{aligned}
u_{\text{e}} &= u_T, & \text{on } \Sigma, \\
\boldsymbol{\sigma}_{\text{e}} \boldsymbol{\nabla} u_{\text{e}} \cdot \mathbf{n} &= \boldsymbol{\sigma}_T \boldsymbol{\nabla} u_T \cdot \mathbf{n}_T, & \text{on } \Sigma.
\end{aligned}
$$

So, we can conclude that the complete bidomain coupled model is:

$$
\begin{aligned}
A_{\text{m}}\big(C_{\text{m}}\partial_t V_{\text{m}} + I_{\text{ion}}(V_{\text{m}}, \mathbf{w})\big) - \operatorname{div}(\boldsymbol{\sigma}_{\text{i}} \boldsymbol{\nabla} V_{\text{m}}) &= \operatorname{div}(\boldsymbol{\sigma}_{\text{i}} \boldsymbol{\nabla} u_{\text{e}}) + I_{\text{app}}, \\
\operatorname{div}((\boldsymbol{\sigma}_{\text{i}} + \boldsymbol{\sigma}_{\text{e}}) \boldsymbol{\nabla} u_{\text{e}}) &= -\operatorname{div}(\boldsymbol{\sigma}_{\text{i}} \boldsymbol{\nabla} V_{\text{m}}), \\
\partial_t \mathbf{w} + \mathbf{g}(V_{\text{m}}, \mathbf{w}) &= 0, \\
\operatorname{div}(\boldsymbol{\sigma}_T \boldsymbol{\nabla} u_T) &= 0,
\end{aligned}
$$

(where the first three equations are in $\Omega_H \times (0, T)$ and the last one in $\Omega_T \times (0, T)$) with border conditions:

$$
\begin{aligned}
\boldsymbol{\sigma}_{\text{i}} \boldsymbol{\nabla} u_{\text{e}} \cdot \mathbf{n} &= -\boldsymbol{\sigma}_{\text{i}} \boldsymbol{\nabla} V_{\text{m}} \cdot \mathbf{n}, & \text{on } \partial\Omega_H = \Sigma \cup \Gamma_{\text{endo}} \\
(\boldsymbol{\sigma}_{\text{i}} + \boldsymbol{\sigma}_{\text{e}}) \boldsymbol{\nabla} u_{\text{e}} \cdot \mathbf{n} &= -\boldsymbol{\sigma}_{\text{i}} \boldsymbol{\nabla} V_{\text{m}} \cdot \mathbf{n}, & \text{on } \Gamma_{\text{endo}} \times (0, T) \\
\boldsymbol{\sigma}_T \boldsymbol{\nabla} u_T \cdot \mathbf{n}_T &= 0, & \text{on } \Gamma_{\text{ext}} \times (0, T)
\end{aligned}
$$

coupling conditions:

$$
\begin{aligned}
u_{\mathrm{T}} &= u_{\mathrm{e}}, & \text{on } \Sigma \times (0,T) \\
(\boldsymbol{\sigma}_{\mathrm{i}} + \boldsymbol{\sigma}_{\mathrm{e}})\boldsymbol{\nabla} u_{\mathrm{e}} \cdot \mathbf{n} &= \boldsymbol{\sigma}_{\mathrm{T}}\boldsymbol{\nabla} u_{\mathrm{T}} \cdot \mathbf{n}_T - \boldsymbol{\sigma}_{\mathrm{i}}\boldsymbol{\nabla} V_{\mathrm{m}} \cdot \mathbf{n}, & \text{on } \Sigma \times (0,T)
\end{aligned}
$$

and initial conditions:

$$
V_{\mathrm{m}}(\mathbf{x},0) = V_{\mathrm{m}}^0(\mathbf{x}), \ \ \mathbf{w}(\mathbf{x},0) = \mathbf{w}^0(\mathbf{x}), \ \ \forall \mathbf{x} \in \Omega_{\mathrm{H}}.
$$

Here we will consider $V_{\mathrm{m}}^0 = V_{\min}$ and $\mathbf{w}^0 = (V_{\max} - V_{\min})^{-2}$.

Finally, to calculate the conductivity tensor in the heart we need to observe that the heart is made of fibers and that the electrical conductivity is higher along the fiber direction than along cross-fiber direction. Intra and extra-cellular media are anisotropic, so we define the conductivity tensor $\boldsymbol{\sigma}_{\mathrm{e}}$ and $\boldsymbol{\sigma}_{\mathrm{i}}$ by:

$$
\begin{aligned}
\boldsymbol{\sigma}_{\mathrm{i}} &= \sigma_{\mathrm{i}}^{\mathrm{t}}\mathbf{I} + (\sigma_{\mathrm{i}}^{\mathrm{l}} - \sigma_{\mathrm{i}}^{\mathrm{t}})\mathbf{a}(x) \otimes \mathbf{a}(x), \\
\boldsymbol{\sigma}_{\mathrm{e}} &= \sigma_{\mathrm{e}}^{\mathrm{t}}\mathbf{I} + (\sigma_{\mathrm{e}}^{\mathrm{l}} - \sigma_{\mathrm{e}}^{\mathrm{t}})\mathbf{a}(x) \otimes \mathbf{a}(x),
\end{aligned}
$$

where $\mathbf{a}(x)$ is a unit vector parallel to the local fiber direction and $\sigma_{\mathrm{x}}^{t}$ and $\sigma_{\mathrm{x}}^{l}$ are respectively the conductivity coefficients measured along the fibers direction and in the transverse direction.

For the conductivity tensor in the thorax we can assume that the thorax has isotropic conductivity: $\boldsymbol{\sigma}_{\mathrm{T}} = \sigma_{\mathrm{T}}\mathbf{I}$ and we take three different values:

$$
\sigma_{\mathrm{T}} = \left\{
\begin{array}{ll}
\sigma_{\mathrm{T}}^{\mathrm{l}} & \text{in lungs,} \\
\sigma_{\mathrm{T}}^{\mathrm{b}} & \text{in bone,} \\
\sigma_{\mathrm{T}}^{\mathrm{t}} & \text{in remaining regions.}
\end{array}
\right.
$$

The constant parameters for $\boldsymbol{\sigma}_{\mathrm{i}}$ and $\boldsymbol{\sigma}_{\mathrm{e}}$ are reported in Table 1.1 and the constants for $\boldsymbol{\sigma}_{\mathrm{T}}$ are reported in Table 1.2 (all expressed in $S\ cm^{-1}$). We will also take $A_{\mathrm{m}} = 200 cm^{-1}$ and $C_{\mathrm{m}} = 10^{-3} mF$.

## 1.3 Ionic current: Mitchell and Schaeffer model

To complete the model we need to define the functions $g$ and $I_{\mathrm{ion}}$ that depend on the considered cell ionic model, i.e. the model that defines the ionic current described in section 1. We consider ionic models with only two state variables: the transmembrane potential $V_{\mathrm{m}}$ and a gate variable $w$. They will reproduce the four phases of a cell polarization and depolarization described above, even if they are not derived from physiological observations. The first model with only two variables that has been proposed is the FitzHugh-Nagumo ([8], [13]) model in 1961. Then, Roger and McCulloch ([20]) and Aliev and Panfilov ([1]) adapted this model to cardiac cells.

- FitzHugh-Nagumo:

$$
I_{\mathrm{ion}}(v,w) = kv(v - a)(v - 1) + w, \ \ g(v,w) = -\epsilon(\gamma v - w).
$$

- Roger-McCulloch:

$$I_{\text{ion}}(v, w) = kv(v - a)(v - 1) + vw, \ g(v, w) = -\epsilon(\gamma v - w).$$

- Aliev-Panfilov:

$$I_{\text{ion}}(v, w) = kv(v - a)(v - 1) + vw, \ g(v, w) = \epsilon(\gamma v(v - 1 - a) + w).$$

The parameters $0 > a > 1$, $k$, $\epsilon$, $\gamma$ are positive constants.

Here, we consider the model proposed by Mitchell and Schaeffer [12] which has been obtained more recently (2003):

$$I_{\text{ion}}(V_{\text{m}}, w) = -\frac{w}{\tau_{\text{in}}}\frac{(V_{\text{m}} - V_{\text{min}})^2(V_{\text{max}} - V_{\text{m}})}{V_{\text{max}} - V_{\text{min}}} + \frac{1}{\tau_{\text{out}}}\frac{V_{\text{m}} - V_{\text{min}}}{V_{\text{max}} - V_{\text{min}}}$$

$$g(V_{\text{m}}, w) = \begin{cases} \dfrac{w}{\tau_{\text{open}}} - \dfrac{1}{\tau_{\text{open}}(V_{\text{max}} - V_{\text{min}})^2}, & \text{if} \ \ V_{\text{m}} < V_{\text{gate}} \\ \\ \dfrac{w}{\tau_{\text{close}}}, & \text{if} \ \ V_{\text{m}} > V_{\text{gate}} \end{cases}$$

(1.9)

where $\tau_{\text{in}}$, $\tau_{\text{out}}$, $\tau_{\text{open}}$, $\tau_{\text{close}}$, $V_{\text{gate}}$, $V_{\text{min}}$ and $V_{\text{max}}$ are the ionic parameters of model. For this model we will refer in all our work to the values in Table 1.3. We see that $\tau_{\text{close}}$ takes different values: $\tau_{\text{close}}^{\text{RV}}$ on the right ventricle and different $\tau_{\text{close}}$ on the left ventricle varying on the transmural direction ($\tau_{\text{close}}^{\text{endo}}$ near the endocardium, $\tau_{\text{close}}^{\text{epi}}$ near the epicardium and $\tau_{\text{close}}^{\text{mcell}}$ in rest of the myocardium). Let us notice that the gate variable $w$ depends on the change-over voltage $V_{\text{gate}}$ and on the time constants of opening and closing of the ionic channels that permit the ionic exchanges (and so, depolarization and repolarization) while the time constants $\tau_{\text{in}}$ and $\tau_{\text{out}}$ are related to the length of depolarization and repolarization phases.

| $\sigma_{\text{i}}^{\text{l}}$ | $\sigma_{\text{e}}^{\text{l}}$ | $\sigma_{\text{i}}^{\text{t}}$ | $\sigma_{\text{i}}^{\text{t}}$ |
|---|---|---|---|
| $3.0 \times 10^{-3}$ | $3.0 \times 10^{-3}$ | $3.0 \times 10^{-4}$ | $1.2 \times 10^{-3}$ |

Table 1.1: Ionic parameters.

| $\sigma_{\text{T}}^{\text{l}}$ | $\sigma_{\text{T}}^{\text{b}}$ | $\sigma_{\text{T}}^{\text{t}}$ |
|---|---|---|
| $2.4 \times 10^{-4}$ | $4 \times 10^{-5}$ | $6 \times 10^{-4}$ |

Table 1.2: Ionic parameters.
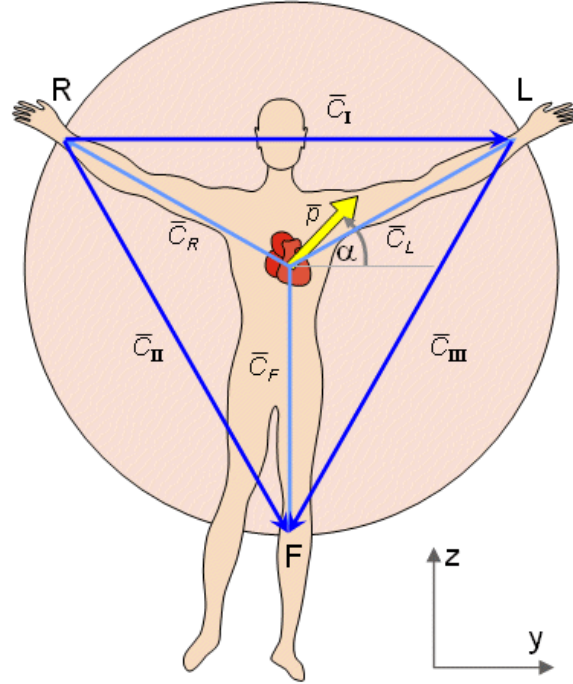
Figure 1.5: Einthoven triangle (Source: bembook [10]).

| $\tau_{\text{in}}$ | $\tau_{\text{out}}$ | $\tau_{\text{open}}$ | $\tau_{\text{close}}$ | $\tau_{\text{close}}^{\text{RV}}$ | $\tau_{\text{close}}^{\text{endo}}$ | $\tau_{\text{close}}^{\text{mcell}}$ | $\tau_{\text{close}}^{\text{epi}}$ | $V_{\text{gate}}$ | $V_{\text{min}}$ | $V_{\text{max}}$ |
|---|---|---|---|---|---|---|---|---|---|---|
| 16 | 360 | 300 | 100 | 120 | 130 | 140 | 90 | $-67$ | $-80$ | 20 |

Table 1.3: Ionic parameters.

## 1.4 Numerical resolution and results

In the whole work we used a weak coupling and the Mitchell and Schaeffer ionic model as illustrated above. The solutions are obtained using a finite element method for the space resolution of equations and a second order BDF (backward differentiation formulae) method for the time discretization. The tool used to obtain the solutions is the C++ LifeV library. More details can be found in [2] and [22].

Once solution of equations (1.7)-(1.8) is computed we need to represent the ECGs. The ECGs are computed according to the standard 12-lead ECG definition:

$$
\begin{array}{ll}
\mathrm{I} = u_\mathrm{T}(L) - u_\mathrm{T}(L) & aVR = \frac{3}{2}(u_\mathrm{T}(R) - u_\mathrm{w}) \\
\mathrm{II} = u_\mathrm{T}(F) - u_\mathrm{T}(R) & aVL = \frac{3}{2}(u_\mathrm{T}(L) - u_\mathrm{w}) \\
\mathrm{III} = u_\mathrm{T}(F) - u_\mathrm{T}(L) & aVF = \frac{3}{2}(u_\mathrm{T}(F) - u_\mathrm{w}) \\
V_1 = u_\mathrm{T}(V_1) - u_\mathrm{w} & V_4 = u_\mathrm{T}(V_4) - u_\mathrm{w} \\
V_2 = u_\mathrm{T}(V_2) - u_\mathrm{w} & V_5 = u_\mathrm{T}(V_5) - u_\mathrm{w} \\
V_3 = u_\mathrm{T}(V_3) - u_\mathrm{w} & V_6 = u_\mathrm{T}(V_6) - u_\mathrm{w}
\end{array}
$$

where $u_\mathrm{w} = (u_\mathrm{T}(L) + u_\mathrm{T}(R) + u_\mathrm{T}(F))/3$ and $L$, $R$ and $F$ indicate different body locations (left and right arm, and right leg, see the Einthoven triangle in Figure 1.5). We report in Figure 1.6 a simulated ECG in an healthy case.
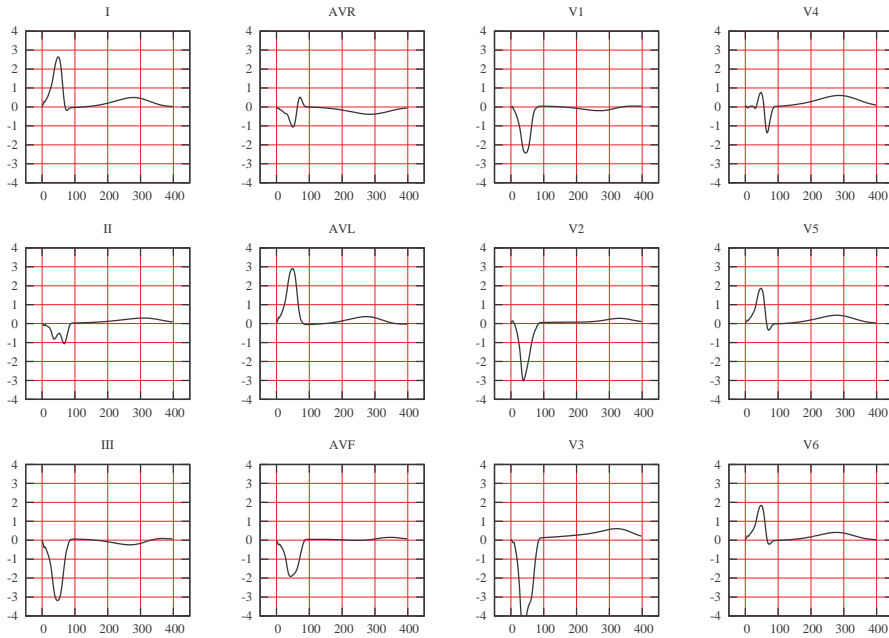


Figure 1.6: Simulated healthy case ECG (time period $= [0, 400]ms$).

### 1.4.1 Applied stimulus

Physiologically, the activation wave begins at the sinusal node in the right atria, it propagates to ventricles through the atrioventricular node and join the endocardium. In the model we used, atria are not included and it is supposed that only endocardium is stimulated. A given volume current density is applied to a thin subendocardial layer of ventricles during a small period of time $t_{\text{act}} = 10ms$. So the source current $I_{\text{app}}$ involved in the model's equations is parametrized as:

$$I_{\text{app}}(x, y, z, t) = I_0(x, y, z)\mathbf{1}_{\text{S}}(x, y, z)\mathbf{1}_{[0, t_{\text{act}}]}(t)\psi(x, z, t),$$

where $S = \{(x, y, z) \in \Omega_{\text{H}} : c_1 \leq ax^2 + by^2 + cz^2 \leq c_2\}$ is the stimulated area, $I_0$ is a function that depends on the coefficient of amplitude $i_{\text{app}}$:

$$I_0(x, y, z) = i_{\text{app}}\Big(\frac{c_2}{c_2 - c_1} - \frac{1}{c_2 - c_1}(ax^2 + by^2 + cz^2)\Big),$$

and $\psi$ is the characteristic function of the activation angle:

$$\psi(x, z, t) = \begin{cases} 1 & \text{if} \quad \text{atan}\big(\frac{x}{z}\big) \leq \alpha(t) \\ 0 & \text{if} \quad \text{atan}\big(\frac{x}{z}\big) > \alpha(t) \end{cases}$$

with $\alpha(t) = \frac{\pi t}{2t_{\text{act}}}$, i.e. only a "cone" which vertex is in the sinusal node is stimulated.

# Chapter 2

# Reduced models

As the resolution of the model presented in Chapter 1 requires a long time[1] we want to solve it using a reduced order model. In general, if we need to solve a numerical problem, the reduced model approach finds a basis that can be used to approximate the solution of the problem. The dimension of the reduced basis is small (typically we will ask to his dimension to be much smaller than the dimension of a finite element basis, i.e. the number of nodes of the mesh).

In our case, we use a method based on the Proper Orthogonal Decomposition (POD). Essentially, POD is a linear procedure that creates an orthogonal base using a given collection of input data. In our case, the input data are the solutions of the problem solved with finite element.

The POD basis we are looking for is made of functions estimated as the solution of an integral eigenvalue problem known as Fredholm equation. From a mathematical point of view, it is strictly based on the Singular Value Decomposition. Basically, this technique allows to extract the most information from a matrix in the most compact way possible. POD approach will be used also in the next chapter that deals with the inverse problem and the parameters identification.

In the next paragraphs we describe the main points of the POD method, for further details see for instance [7].

## 2.1   The Singular Value Decomposition

We first need to introduce the Singular Value Decomposition (SVD). If we consider a full rank matrix $A \in \mathbb{R}^{M \times N}$, $r = \text{rank}(A) = \min(M, N)$, the SVD of $A$ is the factorization

$$A = U \Sigma V^{\dagger}$$

---

[1]It takes about 40 minutes to solve a weak coupling problem of $400 msec$.

where $U$ and $V$ are (non unique) unitary respectively $M \times M$ and $N \times N$ matrices (i.e. $UU^\dagger = I_M$ and $VV^\dagger = I_N$) and the first $r$ lines of $\Sigma$ are $\Sigma_r = \text{diag}(\sigma_1, \ldots, \sigma_r)$, $\sigma_1 \geq \sigma_2 \geq \ldots \geq \sigma_r$ while the last $M - r$ ones are null vectors. The $\sigma_i$ are called singular values of $A$, the first $r$ columns of $U = (u_1, u_2, \ldots, u_M)$ the left singular vectors and the first $r$ columns of $V = (v_1, v_2, \ldots, v_N)$ the right singular vectors.

The SVD is very useful to approximate a matrix with another one which has a specific (smaller) rank. Approximating $A \in \mathbb{R}^{M \times N}$ by a matrix $X$ such that $\text{rank}(X) = k < r = \text{rank}(A)$ is equivalent to solving the minimization problem $\min \|A - X\|$. in a norm that has to be specified. If we consider the Frobenius norm[2], then the solution of this minimization problem is given by the Eckart-Young theorem:

$$\min_{X:\text{rank}(X) \leq k} \|A - X\|_{\text{F}} = \|A - A_k\|_{\text{F}} = \sqrt{\sum_{i=k+1}^{r} \sigma_i^2(A)}, \qquad (2.1)$$

where

$$A_k = U \begin{pmatrix} \Sigma_k & 0 \\ 0 & 0 \end{pmatrix} V^\dagger = \sigma_1 u_1 v_1^\dagger + \ldots + \sigma_k u_k v_k^\dagger,$$

and $\Sigma_k = \text{diag}\{\sigma_1, \ldots, \sigma_k\}$.

This is exactly the idea of the POD: we want to keep from the solution of a finite element problem the most information we can in the most reduced form possible, and use this information to create a basis used which will be used to solve similar problems.

## 2.2 POD method

Generally, when we want to find numerically a solution $u(\mathbf{x}, t)$, depending on space variable $\mathbf{x} \in \Omega$ and on time $t \in [0; T]$, we approximate it by a finite sum in the variable-separated form

$$u(\mathbf{x}, t) \simeq \sum_{k=1}^{K} a_{\text{k}}(t) \phi_{\text{k}}(\mathbf{x}),$$

where the basis functions $\phi_{\text{k}}$ are given a priori. For example they can be Legendre polynomials or Chebyshev polynomials, and the time-functions $a_{\text{k}}$ depend on the choice of the base. In that case, the basis functions are determined independently of the solution to compute. Another possibility is to compute the basis using a collection of data on $u$.

Suppose that we have chosen orthonormal basis functions:

$$\int_\Omega \phi_{\text{k}}(\mathbf{x}) \phi_{\text{l}}(\mathbf{x}) d\mathbf{x} = \delta_{\text{kl}},$$

---

[2]$\|B\|_{\text{F}} = \sqrt{\sum_{i=1}^{n} \sigma_i^2(B)}$ for any $B$ s.t. $\text{rank}(B) = n$

then the coefficients $a_k$, $\forall k = 1, 2, \ldots, K$, only depend on the $k^{\text{th}}$ basis function $\phi_k$ and they are given by:

$$a_k(t) = \int_\Omega u(\mathbf{x}, t)\phi_k(\mathbf{x})d\mathbf{x}.$$

Then the approximation of $u(\mathbf{x}, t)$ can be written as

$$u(\mathbf{x}, t) \simeq \sum_{k=1}^{K} \big(u(\mathbf{x}, t), \phi_k(\mathbf{x})\big)\phi_k(\mathbf{x}),$$

when $(\cdot, \cdot)$ is the $L^2$ inner product. So, if we can measure at $N_t$ different instants of time, $n$ realizations of $u(\mathbf{x}, t)$ in $n$ different locations $x_1, x_2, \ldots, x_n$, the approximation problem is equivalent to solve

$$\min \sum_{i=1}^{N_t} \|u(\mathbf{x}, t_i) - \sum_{k=1}^{K} \big(u(\mathbf{x}, t), \phi_k(\mathbf{x})\big)\phi_k(\mathbf{x})\|_{L^2}^2, \qquad (2.2)$$

i.e. to find the corresponding orthonormal functions $\{\phi_k(\mathbf{x})\}_{k=1}^{K}$ ($K \leq n$).

In practice, we arrange the set of data $\mathcal{U} = \{u(\mathbf{x}, t_1), \ldots, u(\mathbf{x}, t_{N_t})\}$ in a matrix called Snapshot Data Matrix of dimensions $n \times N_t$ with $N_t \leq n$:

$$A = \begin{pmatrix} u(x_1, t_1) & u(x_1, t_2) & \ldots & u(x_1, t_{N_t}) \\ u(x_2, t_1) & u(x_2, t_2) & \ldots & u(x_2, t_{N_t}) \\ \vdots & \vdots & \vdots & \vdots \\ u(x_n, t_1) & u(x_n, t_2) & \ldots & u(x_n, t_{N_t}) \end{pmatrix} \in \mathbb{R}^{n \times N_t}.$$

The snapshots $u(\mathbf{x}, t_i)$ are assumed to be linearly independent, i.e. the data matrix has full column rank. Then the solution of the minimization problem is given by the truncated SVD of length $K$ of $A$.

If we consider a finite element resolution each vector function of $\mathcal{U}$ can be written as

$$u(\mathbf{x}, t_i) \simeq u^n(\mathbf{x}, t_i) = \sum_{j=1}^{n} u^{(j)}(t_i)\varphi^{(j)}(\mathbf{x})$$

i.e. in terms of $n^{\text{th}}$ order finite element basis functions $\{\varphi^{(j)}(\mathbf{x})\}_{j=1}^{n}$. Then, we can define the finite element mass matrix $\mathcal{M} \in \mathbb{R}^{n \times n}$, the associated inner product $(u, v) = \mathbf{u}^{\mathrm{T}}\mathcal{M}\mathbf{v}$ and the $\mathcal{M}$-norm $\|u\|_{\mathcal{M}} = (\mathcal{M}^{1/2}\mathbf{u})^{1/2}$, where $\mathbf{u}, \mathbf{v} \in \mathbb{R}^n$. So we can write the minimization problem (2.2) as

$$\min \sum_{i=1}^{N_t} \|u^n(\mathbf{x}, t_i) - \sum_{k=1}^{K} \big(u^n(\mathbf{x}, t_i), \phi^{(k)}(\mathbf{x})\big)_{\mathcal{M}} \phi^{(k)}(\mathbf{x})\|_{\mathcal{M}}^2 \qquad (2.3)$$

where the POD basis functions $\{\phi^{(k)}(\mathbf{x})\}_{k=1}^{K}$ are assumed to be in the linear space spanned by the finite element functions $\{\varphi^{(j)}(\mathbf{x})\}_{j=1}^{n}$:

$$\phi^{(k)}(\mathbf{x}) = \sum_{j=1}^{n} \phi_j^{(k)}\varphi^{(j)}(\mathbf{x}).$$

We can find out that the minimization problem (2.3) can be written in matrix representation as

$$\min_{Z \in \mathbb{R}^{n \times K} : Z^{\mathrm{T}} Z = I_K} \|\hat{A} - Z Z^{\mathrm{T}} \hat{A}\|_{\mathrm{F}}^2, \text{ s.t. } Z Z^{\mathrm{T}} = I_K \qquad (2.4)$$

where $\hat{A} = (\mathcal{M}^{1/2})^{\mathrm{T}} A$, $Z = (\mathcal{M}^{1/2})^{\mathrm{T}} \Phi \in \mathbb{R}^{n \times K}$, $\Phi \in \mathbb{R}^{n \times K}$ is the matrix collecting the finite element coefficients of the unknown POD functions. We can summarize that we are looking for a $K$ dimensional subspace $\Phi$ such that $X = Z Z^{\mathrm{T}} \hat{A}$ is the best approximation to $\hat{A}$ compared with all subspaces of dimension $K$. Then, thanks to Eckart-Young theorem (2.1), the solution is given by the truncated SVD of $\hat{A} = (\mathcal{M}^{1/2})^{\mathrm{T}} A$ of length $K$:

$$\hat{A}_K = U_K \Sigma_K V_K^{\mathrm{T}}$$

where $\Sigma_K = \mathrm{diag}\{\sigma_1, \ldots, \sigma_K\}$ is the diagonal matrix of the first $K$ singular value of $\hat{A}$, $U_K$ corresponds to the first $K$ columns of $U$ and $V_K$ to the first $K$ columns of $V$. Finally, comparing $\hat{A}_K$ and $X$, we can find that $\Phi$ solves:

$$(\mathcal{M}^{1/2})^{\mathrm{T}} \Phi = U_K \in \mathbb{R}^{n \times K} \in \mathbb{R}^{n \times K}.$$

The coefficients of the POD basis functions can be found solving this system, where we can obtain the left singular vectors $U$ of $\hat{A} = U \Sigma V^{\mathrm{T}}$ computing the eigenvalues of the matrix $\hat{A}\hat{A}^{\mathrm{T}} \in \mathbb{R}^{n \times n}$ (or, as $N_t \ll n$, we can compute the right singular vectors $V$ of the matrix $\hat{A}^{\mathrm{T}}\hat{A} \in \mathbb{R}^{N_t \times N_t}$).

# Chapter 3

# Inverse problem resolution

## 3.1 Optimization method

Our aim is to identify $N$ parameters of the problem by comparing the corresponding ECG to the reference one, i.e. we want to find the parameters that give the closest ECG compared to the reference one. If we consider a subset $I \subset \mathbb{R}^N$ of parameters we look for the $j^* \in I$ that minimizes the function:

$$\Psi(j) = \delta t \sum_{i=1}^{N_t} \left( |\mathrm{I}^{(j)}(t_i) - \mathrm{I}^{(\mathrm{ref})}(t_i)|^2 + |\mathrm{II}^{(j)}(t_i) - \mathrm{II}^{(\mathrm{ref})}(t_i)|^2 + \ldots \right.$$

$$\left. \ldots + |V_6^{(j)}(t_i) - V_6^{(\mathrm{ref})}(t_i)|^2 \right)$$

where $\mathrm{I}^{(j)}$, ..., $V_6^{(j)}$ are the leads of the ECG associated to the solution corresponding to the set of parameters $j$ in $I$ and $\mathrm{I}^{(\mathrm{ref})}$, ..., $V_6^{(\mathrm{ref})}$ are those of the reference one. Finally, the problem we need to solve is:

$$j^* = \arg \min_{j \in I} \Psi(j).$$

To solve this optimization problem we use a genetic algorithm. In general genetic algorithms are heuristic methods to find the solution of an optimization problem: an initial population is created and manipulated using techniques inspired by natural genetic evolution such as mutation, selection and crossover. At each iteration of the algorithm, the population members, i.e. the solutions of the problem, are evaluated, a part of them is saved and other members are generated. Finally, the solution is taken as the best one of the population. In section 3.2 and 3.3 we can find more details about the algorithm we used. Genetic algorithms can also be very easily executed in parallel: at each generation each member of the population can be evaluated in parallel compared with the others. So if we run our algorithm, for instance, on a 8 processors computer we can calculate the cost function, i.e.

solve the bidomain problem, of 8 points at the same time and divide the computational time by 8.

## 3.2 Genetic Algorithms

In general, a genetic algorithm follows the evolution of a population, i.e. a number $N_{\mathrm{p}}$ of possible solutions. Each individual $j \in I$ of the population is evaluated compared with the function that has to be minimized $\Psi(j)$. The genetic algorithm is iterative and at each of the $N_{\mathrm{g}}$ iterations a new population of size $N_{\mathrm{p}}$ is generated by modifying the previous one and it is added to the total population. The regeneration of a population is made by using selection, crossover and mutation that are stochastic principles based on the "survival of the fittest" biological laws.

At each iteration a new population $X_{\mathrm{new}}$ is created, collecting randomly existing members of the previous population, then selection is applied to these units. Selection consists in choosing randomly $N_{\mathrm{p}}/2$ couples of the new population $X_{\mathrm{new}}$. Crossover and mutation are applied to each couple.

Crossover consists in creating two new elements starting from those of the selected couple. It takes a barycentric combination of them with random and independent coefficients (see Algorithm 1).

---
**Algorithm 1** Crossover
---
**for** each couple $X(i), X(i+1)$ **do**
    $u =$ random coefficient $\in [0, 1]$
    $X_{\mathrm{new}}(i) = uX(i) + (1-u)X(i+1)$
    $X_{\mathrm{new}}(i+1) = uX(i+1) + (1-u)X(i)$
**end for**

---

Mutation replaces randomly a member of the population by one of its neighbors, where neighbor indicates an element of the population similar to the considered one: in the case of a real parameter it is a perturbation of its value (see Algorithm 2).

---
**Algorithm 2** Mutation
---
**for** each member of the population $X(i)$ **do**
    $u_1 =$ random coefficient $\in [0, 1]$
    $u_2 =$ random coefficient $\in [0, 1]$
    **if** $u_1 < 1/2$ **then**
        $X_{\mathrm{new}}(i) = X(i) + u_2(X_{\mathrm{max}} - X(i))$
    **else**
        $X_{\mathrm{new}}(i) = X(i) - u_2(X(i) - X_{\mathrm{min}})$
    **end if**
**end for**

---

To be sure to keep the most suitable solutions there is also a one-elitism principle. Once the new population is created and each new member has been evaluated with respect to the objective function, the elitism keeps into the new population to be build the best solution still found, so that mutation will introduce elements near this one.

The genetic algorithm can be written as in Algorithm 3, for further details we can refer to [5].

---

**Algorithm 3** Genetic Algorithm

---

Choice an initial population $P_1 \subset I$ s.t. $\forall x \in P_0, x_i \in [x^i_{\min}, x^i_{\max}]$
$n_g = 1$
**while** $n_g < N_g$ **do**
   evaluate $\Psi(x) \; \forall x \in P_{n_g}$
   $m = \min_{x \in P_{n_g}} \Psi(x)$
   $X_{n_g} = \arg\min_{x \in P_{n_g}} \Psi(x)$
   **elitism** :
   **if** $n_g > 2$ and $J(X_{n_g-1}) < m$ **then**
      $x^i_{n_g} = X_{n_g}$ for a random $i$
   **end if**
   **for** k from 1 to $N_p/2$ **do**
      **selection** of $(x^\alpha_{n_g}, x^\beta_{n_g})$
      replace $(x^\alpha_{n_g}, x^\beta_{n_g})$ with $(y^\alpha_{n_g}, y^\beta_{n_g})$ by **crossover**
      replace $(y^\alpha_{n_g}, y^\beta_{n_g})$ with $(z^\alpha_{n_g}, z^\beta_{n_g})$ by **mutation**
   **end for**
   $n_g = n_g + 1$
   $P_{n_g} = P_{n_g} \bigcup X_{\text{new}}$
**end while**
**return** $X = \arg\min_{x \in P_{N_g}} \Psi(x)$

---

## 3.3 Approximated Genetic Algorithm

As the computation of the exact evaluation of the objective function is very expensive (we remember that it is the resolution of the bidomain model for a one beat time period), we can use an approximated evaluation of $\Psi$ for some members of the population. Particularly, the objective function is evaluated exactly for the first $N_{\text{exac}}$ population, then the number of exact evaluations at each iteration decreases with a rate $r \in (0, 1)$. The approximated functions are computed with an interpolation method called Radial Basis Function (RBF) interpolation. The idea of the RBF interpolation is to make a linear combination of $\Psi$ in $b$ the nearest points.

# Part II

# The myocardial infarction

# Chapter 4

# Simulation of a myocardial infarction

Heart attacks are one of the leading causes of death for both men and women worldwide. The myocardial infarction (also called heart attack) is the consequence of the occlusion of a coronary artery, that causes a deficit of blood in an heart region (ischemia). If the ischemia is left untreated during a long period of time, it can cause an infarction (damage or death of part of the myocardium). One of the tests that can be used to detect heart muscle damage is the ECG.

There are two main kinds of myocardial infarctions: transmural and subendocardial. The last ones involve only a small area in the subendocardial wall of the left ventricle, while the transmural ones are usually result of a complete occlusion of area's blood supply and they extend through the whole thickness of the heart muscle. We will only consider transmural infarctions, that can be classified into posterior, anterior, lateral and inferior. Moreover, we will focus on infarction in the left ventricle because usually the infarction is located in the left ventricle, that is thicker than the right one.

## 4.1 Modeling of an infarction

A way to simulate this pathology is to act on $\tau_{\text{out}}$, the ionic parameter of the Mitchell and Schaeffer model (see section 1.3) related to the repolarization phase length. To simulate this heart tissue damage we can modify the constants $\tau_{\text{in}}$ and $\tau_{\text{out}}$ that govern the length of depolarization and repolarization phases in a restricted area where the infarction is assumed to be located, defined as:

$$S_{\text{inf}} = \{(x, y, z) \in \Omega_{\text{H}} : (x - x_0)^2 + (y - y_0)^2 + (z - z_0)^2 \leq r^2\},$$

where $(x_0, y_0, z_0)$ is a point of the left ventricle epicardium.

If we modify the constants $\tau_{\mathrm{in}}$ and $\tau_{\mathrm{out}}$ in $S_{\mathrm{inf}}$, this area will be depolarized and repolarized in a different way.

In an infarcted area of the heart, there is an increase of the extra-cellular concentration of ions $K^+$ ($[K^+]_{\mathrm{o}}$) as explained in details in [15]. As said in the introduction, the heart tissue can not conduct any more, this leads to a lack of oxygen and consequently to a reduction of ATP production (see section 1). The deficiency of ATP prevents the $Na/K$ pump to be activated, so the flux of ions $K^+$ and the associated current are negligible. As a consequence, all the phases of the polarization cycle are modified.

So, as in repolarization phase an active exchange occurs, i.e. with expenditure of energy, we decide to act on the associated current and, as a consequence, the others phase will be modified. Particularly, we decide to act only on $\tau_{\mathrm{out}}$, even if a similar manipulation can be done with good results also on $\tau_{\mathrm{in}}$ (see section 4.3).

Our aim is to reduce the $K^+$ current due to the pump activation, that is an inward current. We recall that the ionic current used in the Mitchell and Schaeffer model (1.9) is:

$$I_{\mathrm{ion}}(V_{\mathrm{m}}, w) = -\frac{w}{\tau_{\mathrm{in}}}\frac{(V_{\mathrm{m}} - V_{\mathrm{min}})^2(V_{\mathrm{max}} - V_{\mathrm{m}})}{V_{\mathrm{max}} - V_{\mathrm{min}}} + \frac{1}{\tau_{\mathrm{out}}}\frac{V_{\mathrm{m}} - V_{\mathrm{min}}}{V_{\mathrm{max}} - V_{\mathrm{min}}}.$$

It is easy to see that there is a negative term ($I_{\mathrm{in}} = -\frac{w}{\tau_{\mathrm{in}}}v^2(1 - v)$, where $v = (V_{\mathrm{max}} - V_m)/(V_{\mathrm{max}} - V_{\mathrm{min}})$) that corresponds to the inward current, and a positive one ($I_{\mathrm{out}} = \frac{v}{\tau_{\mathrm{out}}}$) that corresponds to the outward current. So it is sufficient to decrease the value of $\tau_{\mathrm{out}}$ in $S_{\mathrm{inf}}$ to make the outward current prevailing on the inward one.

If we simulate an anterior infarction[1] with this technique we find the results showed in Figure 4.1: the value of $\tau_{\mathrm{out}}$ is divided by ten compared with the healthy case ($\tau_{\mathrm{out}}^{\mathrm{inf}} = 36$). We can see that the infarcted area is well defined and stays completely polarized during all the beat. So, enforcing the repolarization phase is sufficient to modify the whole cycle of the infarcted cells and well simulate an infarction.

---

[1]The center of the anterior infarct has coordinates $(x_0, y_0, z_0) = (5.49930 \times 10^{-1}, -3.86215, -1.12360)$
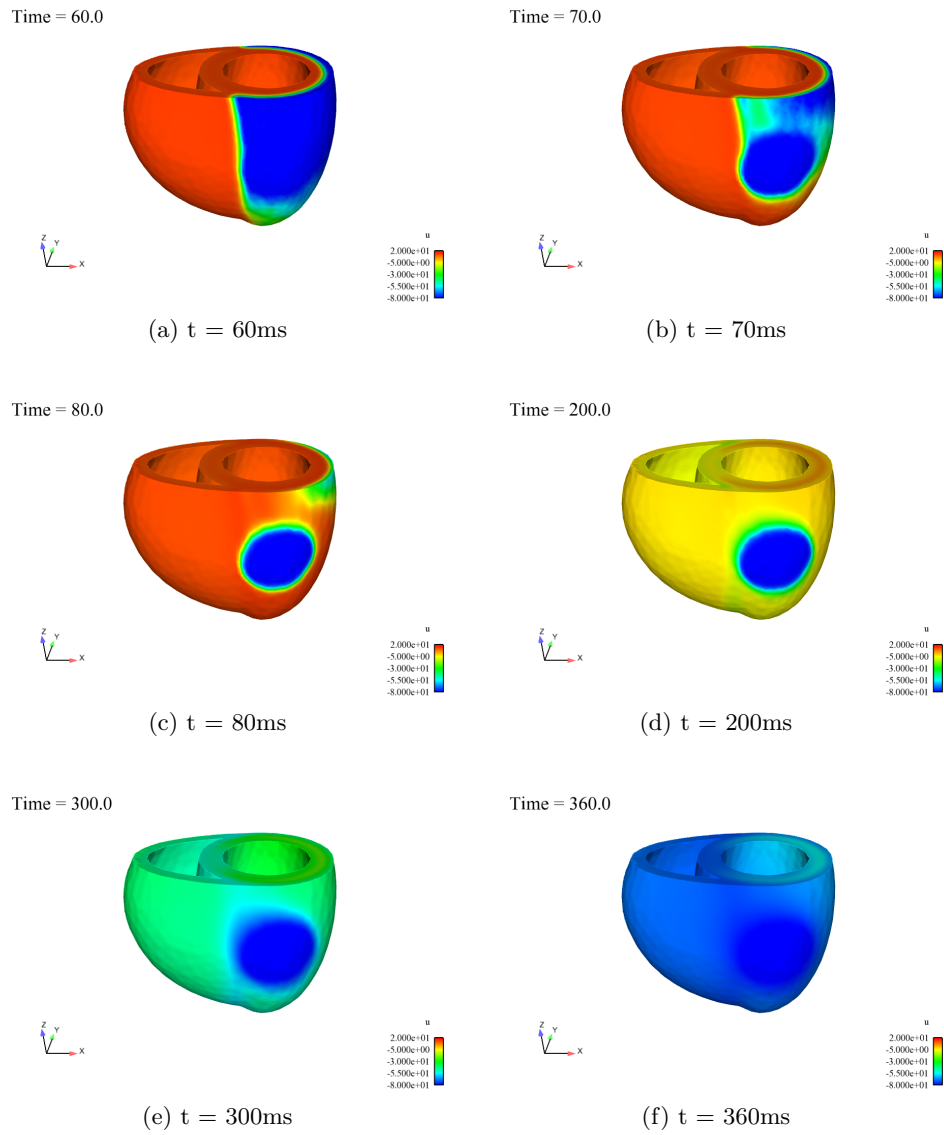
(a) t = 60ms

(b) t = 70ms

(c) t = 80ms

(d) t = 200ms

(e) t = 300ms

(f) t = 360ms

Figure 4.1: Depolarization and repolarization phases of an anterior infarction generated by modifying the value of $\tau_{\text{out}}$.

## 4.2   Simulation of ECG with infarction

As said above, one of the tests used to detect a myocardial infarction is the ECG. The main observation in a real ECG when infarction occurs is a elevation or depression of the ST segment in different leads. More details of an infarction consequences can be find for instance in [4]. The main features we should find are:

- in the case of a posterior infarction: a depression in the ST segment in the $V_1$ and $V_2$ leads;

- in the other cases: an elevation in the ST segment with an inverted T wave;

- in the case of an anterior infarction we should look at $V_1, V_2$ or $V_3$, in the case of a lateral one I or $aVL$ and for an inferior one to II, III or $aVF$.

Finally, in the case of a recent infarction we can also find a Q wave.

Many studies have been conducted to investigate the consequences of an infarction on the ECG, but it is still not fully understood. The main ECG observation that conducts to the diagnosis of infarction is ST elevation or depression.

The main cause of ST elevation (or depression) is exactly the myocardial ischemia, particularly [16], [17], [18] explain this elevation or depression as a consequence of the increased concentration of $K^+$ in the extra-cellular domain ($[K^+]_o$). Increasing $[K^+]_o$ leads to a less negative resting transmural potential $V_m$ and to a reduction of the action potential duration (APD). A higher resting $V_m$ and a decreased APD cause a lower plateau potential at cell scale, that leads to an ST elevation or depression depending on the lead we consider and its position with respect to the infarcted area, as explained above. So, a technique to simulate an infarction in the case of the use of a physiological model could be to modify the transmural potential values in the infarcted area, while in this work we prefer act on the ionic current because of the chosen models.

With the technique described above, we simulate the four kinds of infarction mentioned, the results we find are summarized in Figures 4.2 and 4.3. Looking at the $V_1$ lead, as expected, we can see that the posterior infarction (blue line in Figure 4.2) presents a depression in the ST segment compared with the healthy case (black line), while the anterior one (green line) presents an elevation. Also in the $V_2$ lead we find an elevation for the anterior infarction and we can see no differences with the healthy case in $V_3$, while the posterior one presents depression in both $V_2$ and $V_3$ leads.

If we look at the lateral infarction (green line in Figure 4.3) we find out that there are elevations in the first lead I and in the $aVL$ as expected.
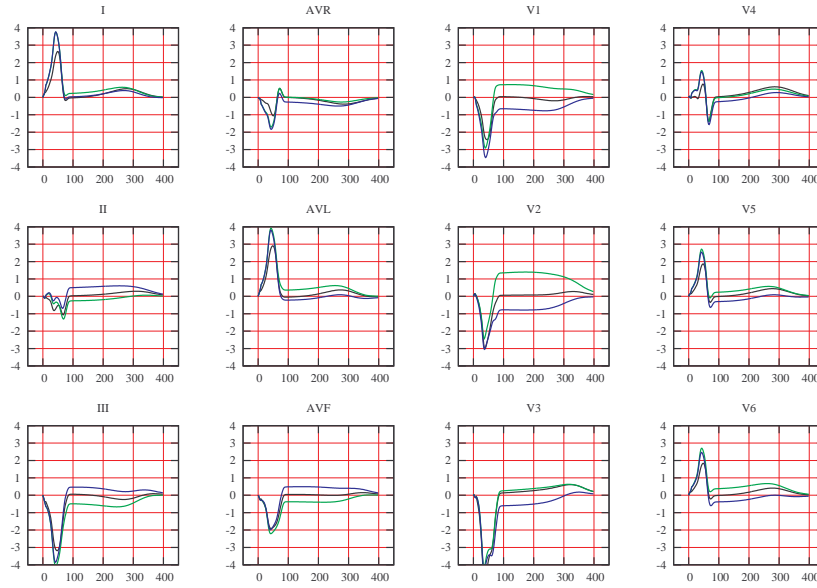
Figure 4.2: Simulated ECGs for different infarcted zones: green line corresponds to an anterior infarction, blue line to a posterior infarction (time period $= [0, 400]ms$). Black line represents the healthy case of reference.
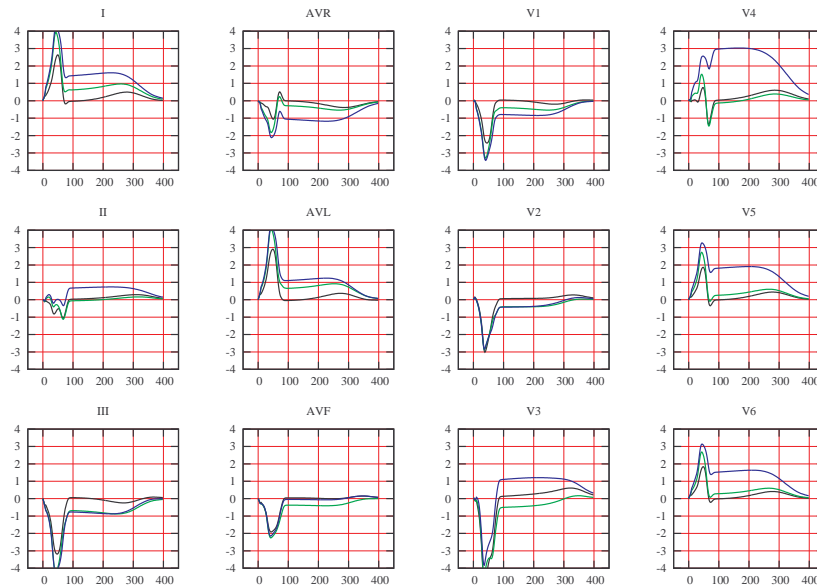


Figure 4.3: Simulated ECGs for different infarcted zones: green line corresponds to a lateral infarction, blue line to an inferior infarction (time period $= [0, 400]ms$). Black line represents the healthy case of reference.

Finally, we point out that the inferior infarction (blue line) is the worst one to simulate: we do not notice any difference in $aVF$ lead and we find a sub-elevation instead of an over-elevation in the third lead (III), but we have a good result in II where we see an elevation of ST. At the same time, we can observe that strong elevations (about $2mV$) occur in the pericordial leads $V_3, V_4, V_5$ and $V_6$. The problems we found simulating inferior infarction are probably due to the fact that it is located near the stimulation area.

## 4.3   Remarks

The modification of the $\tau_{\text{out}}$ parameter is not the only way to simulate an infarction, as mentioned above we can also act on the $\tau_{\text{in}}$. We can also notice that we can simply modify the conductivity coefficients to have quite good results. Here is a brief description of these techniques.

### Reduction of the inward current

As notice in section 4.1, the most important phase, i.e. the phase we are induced to force, is the repolarization one because of its active nature. We also noticed that, to decrease the $K^+$ inward current generated by the $Na/K$ pumps, the outward current $I_{\text{out}}$ corresponding to $Na^+$ has to be dominant. So, an alternative choice that can be done is to augment the $\tau_{\text{in}}$ in the infarcted zone $S_{\text{inf}}$ such that $|I_{\text{ion}}| \simeq |I_{\text{out}}|$. Particularly, simulations shows that it is sufficient to multiply $\tau_{\text{in}}$ by 10 to obtain good results.

On the left column of of Figures 4.4, we have represented some snapshots of the heart potential in the case of a posterior infarction modeled by a reduction of the inward current, i.e. the value of $\tau_{\text{in}}$. During the depolarization phase (approximately the first $100ms$ after the stimulation, first and second rows) we notice that the infarcted area is less sharp than in the previous case and it is subjected to a partial depolarization, this happens because during depolarization phase there is only the inward current due to the $Na$ ionic channel, while the outward current previously modified does not play any role. During repolarization phase too (see Figure 4.4c) we can notice few differences, even if negligible.

### Conductivity coefficients

As observed, an infarction induces a non-depolarization of an heart's area. To simulate this heart tissue damage we can simply modify the coefficients of the conductivity tensor $\boldsymbol{\sigma}_{\text{i}}$, $\boldsymbol{\sigma}_{\text{e}}$ described in chapter 1. In $S_{\text{inf}}$ we put $\sigma_{\text{i}}^{\text{l}}$, $\sigma_{\text{i}}^{\text{t}}$, $\sigma_{\text{e}}^{\text{l}}$ and $\sigma_{\text{e}}^{\text{t}}$ to zero (in fact their values will be $10^{-13}$ in order to keep the coercivity of the problem).

We can see in the right column of hearts of Figure 4.4 the evolution of the depolarization and repolarization phases at different time steps in the case
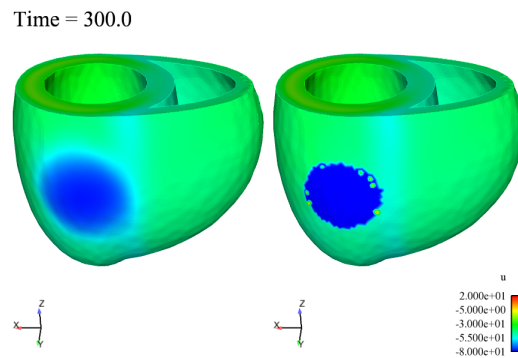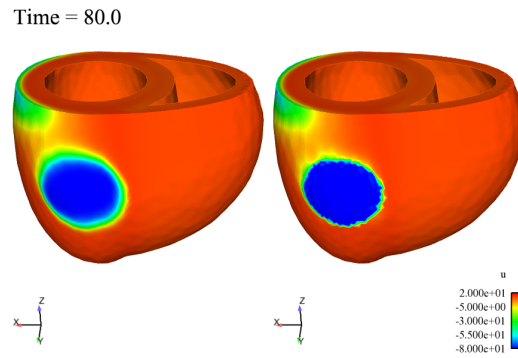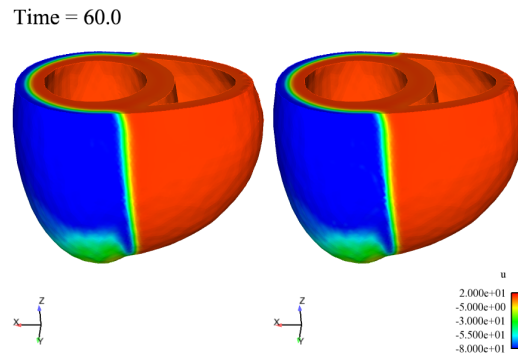
Time = 60.0

(a) t = 60ms

Time = 80.0

(b) t = 80ms

Time = 300.0

(c) t = 300ms

Figure 4.4: Depolarization and repolarization phases of a posterior infarction generated by modifying the ionic parameter $\tau_{in}$ (left) or the conductivity constants (right).

of a posterior infarction obtained by modifying the conductivity coefficients. First we can see that, when we modify the conductivity, the infarction area is better defined, its border is less regular than in the previous cases but the interested area remains completely polarized for the whole period.

Also if we look at the ECG simulated with the three techniques (Figure 4.5) we notice that there are only slight differences even if the increasing outward current seems to be a better method to reproduce the ST elevations and depressions expected.
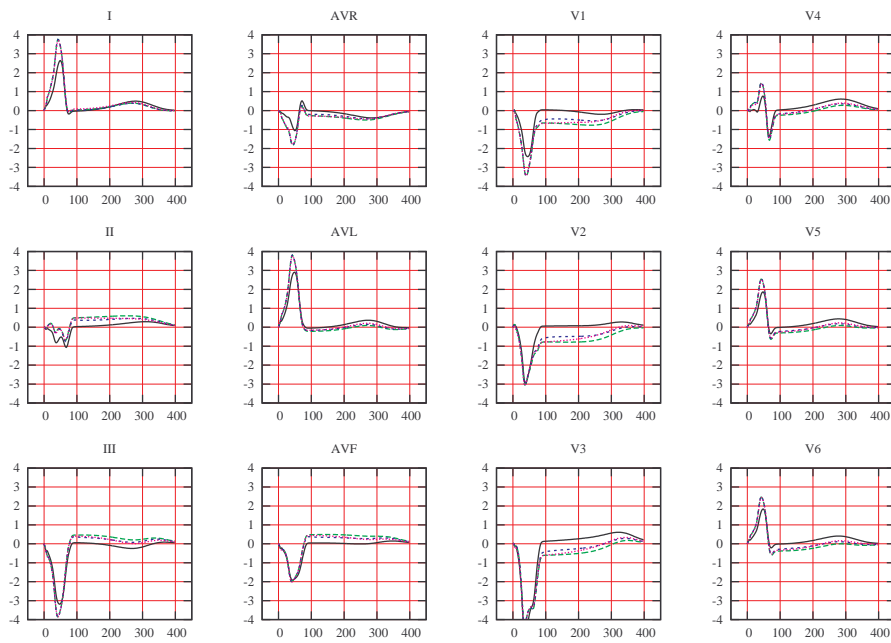


Figure 4.5: Simulated ECGs with different infarction simulation techniques for a posterior infarction: green line corresponds to the modification of $\tau_{\mathrm{out}}$, blue line to the modification of $\tau_{\mathrm{in}}$ and the pink one to the conductivity coefficients (time period $= [0, 400]ms$). Black line represents the healthy case of reference.

# Chapter 5

# Application of the POD

Our aim is now to use a reduced model in order to simulate different kinds of infarction. Particularly we would like to build a unique POD basis which can be used to solve a problem with a generic infarction point (not only the four mentioned in the last chapter). To do so, we will simply apply the tools described in chapter 2. Then we will use genetic algorithms described in chapter 3 to solve the inverse problem of finding the infarcted center looking at the simulated ECG. At each iteration of the genetic algorithm the POD method will be used to reduce the computational time of the resolution of the direct problem.

## 5.1 Numerical simulation with a reduced model: first approach

The first approach to simulate a transmural myocardial infarction with the POD method is to use a basis generated from the resolution of the problem in a healthy case. Let us consider an anterior infarction for which we expect an ST elevation in $V_1$, $V_2$ or $V_3$ leads. As in chapter 4, we impose an heterogeneous $\tau_{\mathrm{out}}$ to simulate the infarction and we use a reduced model: we take the POD basis generated from the numerical simulation of an healthy case. The results we find are shown in Figure 5.1: the simulation with the reduced model is unable to reproduce the infarction. The POD basis "impose" an homogeneous transmembrane potential even if we are trying to simulate a discontinuous one, while the heterogeneous $\tau_{\mathrm{out}}$ modify the infarcted area increasing the repolarization phase.

Also looking at the ECG in Figure 5.2 we notice that the reduced model built on the healthy case (green line) is unable to reproduce the pathology: the ECG has the same shape as the healthy case (black line) and it is not able to reproduce the ST elevation or depression of the complete model simulated infarction (blue line). We also notice that the T wave in the case of POD application is much greater than the healthy ECG.
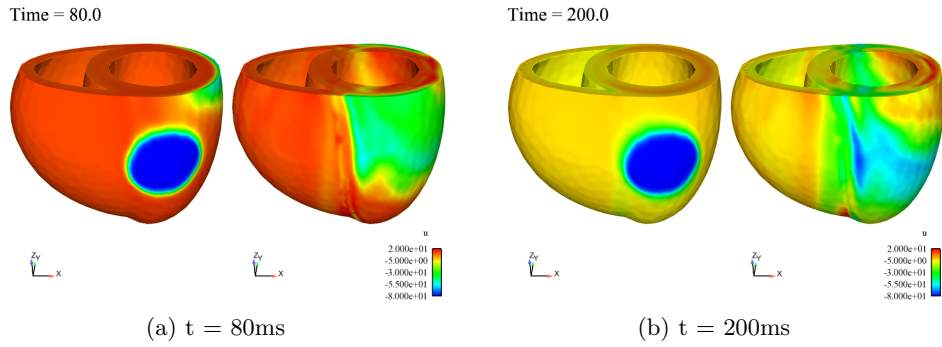
(a) t = 80ms                                        (b) t = 200ms

Figure 5.1: Simulated anterior infarction: comparison between the complete model solution (left) and the "healthy" POD reduced model one.
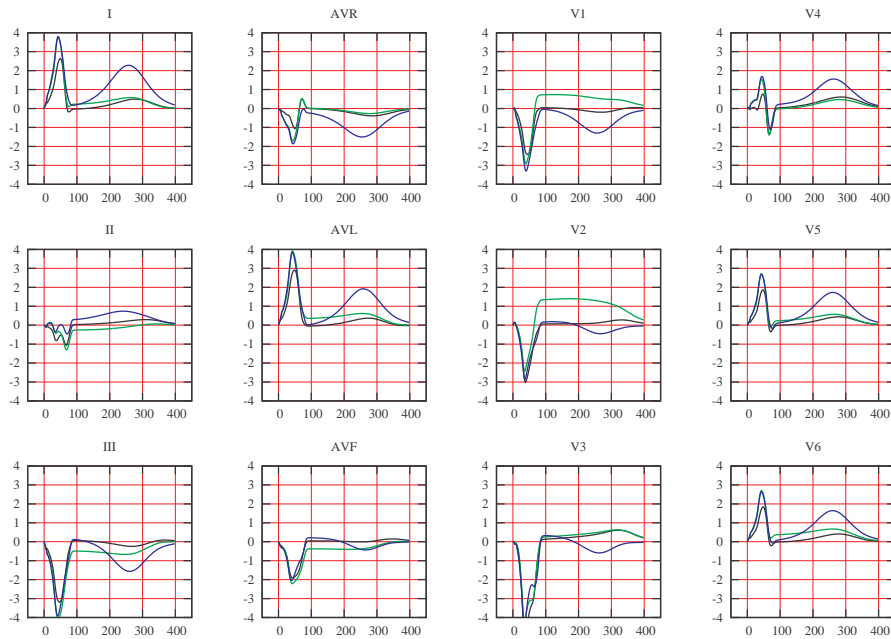


Figure 5.2: Simulated ECG for an anterior infarction: black line represents the healthy case ECG, green one corresponds to the complete model simulated infarction and blue one to the "healthy POD" reduced solution.

A second approach could be to build the POD basis using the numerical solution of an anterior infarction to simulate both an anterior or a posterior ones. This approach obviously produces excellent results for the anterior one while does not approximate the posterior one. In the next section we will propose methods to construct enriched POD basis and this will allow to get round this problem.

## 5.2 Numerical simulation with POD method: improvement

As exposed in [3] different techniques can be applied when parameters vary. The first one is to compute many POD basis for different values of the parameters, in this case different infarcted points, and then use the POD basis corresponding to the closest infarcted center already computed to solve a generic infarction problem. The second approach they propose is to store the solutions of a set of problems, i.e. of different infarcted centers, and build a unique snapshots matrix $A$ collecting all the solutions: the POD basis is then obtained with a SVD on this composed matrix. Here, we present the second approach as a reasonable solution: even if the snapshots matrix has a lot of columns, its SVD has to be calculated once for all. We will see that only 100 modes of the SVD of $A$ are sufficient to reproduce a generic infarction.

The first step is to simulate infarctions located at different positions such that the whole of the external left ventricle surface can be covered. So, we build a kind of coarse mesh on the left ventricle epicardium and we choose 18 infarction points as in Figure 5.6 (which coordinates are expressed in Table 5.1) and we solve these problems without using POD reductions. The results we find are then used to build the POD basis.

We will create a snapshots matrix $\mathcal{U}$ (see chapter 2) containing snapshots $u_p(\mathbf{x}, t_i)$, $p = 1, 2, \ldots, 18$, $i = 0, 1, 2, \ldots, 200$[1], extracted from the different infarction problems described above and also from the healthy case problem. Particularly we decide to extract 100 snapshots from the healthy problem and 50 snapshots from each infarction one. As we know that most of the solutions variation occurs during the first $100msec$ we decide to keep half of the total snapshots in this period, i.e. for the healthy problem we keep $u(\mathbf{x}, t_0)$, $u(\mathbf{x}, t_2)$, ..., $u(\mathbf{x}, t_{48})$, $u(\mathbf{x}, t_{50})$, $u(\mathbf{x}, t_{56})$, ..., $u(\mathbf{x}, t_{194})$ while for each infarction problem we keep $u(\mathbf{x}, t_0)$, $u(\mathbf{x}, t_4)$, ..., $u(\mathbf{x}, t_{48})$, $u(\mathbf{x}, t_{50})$, $u(\mathbf{x}, t_{62})$, ..., $u(\mathbf{x}, t_{194})$. Then we write a snapshots matrix $\mathcal{U}$ which dimensions are $N_{\text{nodes}} \times 1000$. We finally set the POD basis dimension to $K = 100$, i.e. we keep the truncated SVD of $\mathcal{U}$ of length $K$.

---

[1]We remind that the time variable $t \in [0, 400]msec$, we solve the problem with a time step of $\Delta t = 0.5msec$ and we save the solutions each 4 iterations, i.e. each $2msec$. So $t_0 = 0ms$, $t_1 = 2ms$, $t_2 = 4ms$, ..., $t_{200} = 400ms$.

|          | $x$                          | $y$                          | $z$                          |
|----------|------------------------------|------------------------------|------------------------------|
| point a  | $-9.70328 \times 10^{-2}$    | $-3.84531$                   | $-1.66581$                   |
| point b  | $-9.19247 \times 10^{-02}$   | $-3.25782$                   | $-4.024400$                  |
| point c  | $-9.70332 \times 10^{-02}$   | $-2.36176$                   | $-5.71067$                   |
| point d  | $-9.70330 \times 10^{-02}$   | $-3.95123$                   | $8.02269 \times 10^{-1}$     |
| point e  | $2.69873$                    | $-2.84974$                   | $8.21607 \times 10^{-1}$     |
| point f  | $2.69354$                    | $-2.74906$                   | $-1.66581$                   |
| point g  | $2.69293$                    | $-1.82947$                   | $-4.03178$                   |
| point i  | $2.36941$                    | $-5.46018 \times 10^{-3}$    | $-5.71558$                   |
| point l  | $3.84298$                    | $-5.46018 \times 10^{-3}$    | $-1.67281$                   |
| point m  | $3.83000$                    | $-9.52023 \times 10^{-1}$    | $8.04630 \times 10^{-1}$     |
| point n  | $3.83142$                    | $9.57373 \times 10^{-1}$     | $8.04390 \times 10^{-1}$     |
| point o  | $2.70480$                    | $2.87882$                    | $8.04390 \times 10^{-1}$     |
| point p  | $2.69992$                    | $2.74469$                    | $-1.66581$                   |
| point q  | $2.70503$                    | $1.87246$                    | $-4.02440$                   |
| point r  | $-9.70330 \times 10^{-2}$    | $3.95074$                    | $7.96123 \times 10^{-1}$     |
| point s  | $-9.70330 \times 10^{-2}$    | $3.84690$                    | $-1.67340$                   |
| point t  | $-9.76190 \times 10^{-2}$    | $3.26934$                    | $-4.02440$                   |
| point u  | $-9.70331 \times 10^{-2}$    | $2.39998$                    | $-5.71810$                   |

Table 5.1: Coordinates of the infarction points used to build the POD base.

Once the POD basis functions are obtained, we first check that we can find exactly the same solution if we use this basis for one of the infarction problems used to build the basis. If we compare the ECGs obtained using POD and the ones obtained with the complete model (respectively blue line and green one in Figure 5.3 for the "point a" infarction case) we can see that they are exactly superimposed, even if the basis is composed of snapshots of several simulations. This result implies that, even if we keep only few snapshots for each simulated infarction, the POD takes into account enough information to reproduce each one of these solutions.

Next we also would like to apply our POD basis to a generic infarction point problem different from any of the points mentioned above. Let us consider the arbitrary point $w^2$ indicated by the arrow in Figure 5.6 and let

---

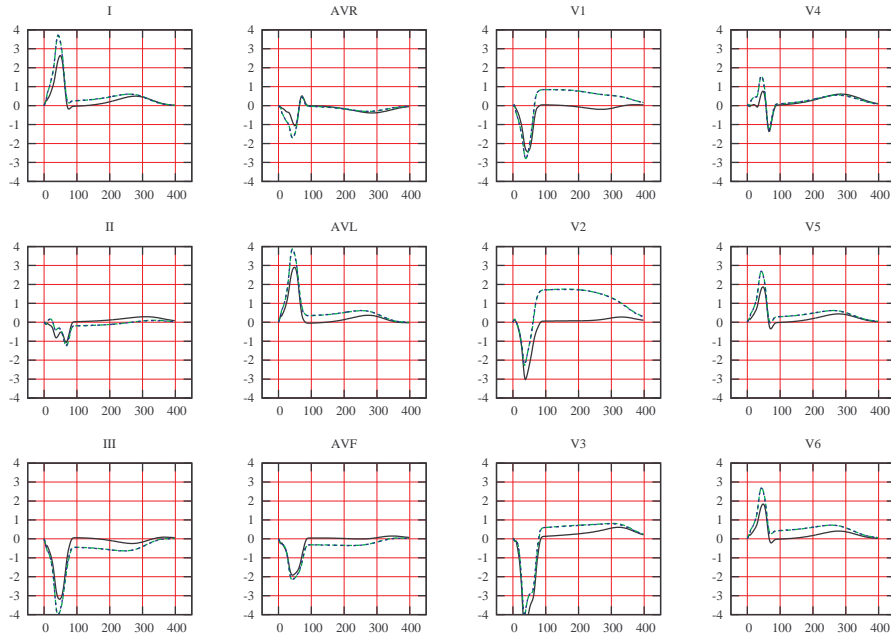[2]The coordinates of this point are $w = (1.53154, -3.34528, -2.70672)$.

Figure 5.3:  Simulated ECG for an infarction centered in point $a = (-9.70328 \times 10^{-2}, -3.84531, -1.66581)$: in black the healthy case ECG, in green the ECG obtained modifying the $\tau_{\text{out}}$ with the complete model and in blue the ECG obtained using the reduced model (always modifying $\tau_{\text{out}}$).

us compare the results obtained without using POD and the results with POD method (respectively green and blue line of the corresponding ECGs in Figure 5.4). If we look at the resulting ECGs, we can see that the curve trend is similar but there is a considerable difference in magnitude: the ECG coming from the POD in most leads has ST segment more elevated or depressed than the one obtained with the complete model. To better understand this result we can look at the transmembrane potential: if we plot it in the whole domain of the heart (Figure 5.5, on top, the solution of the complete model and, on the left, the solution of the POD model) we can see the influence of the POD approach. While with the complete model the infarcted area is well defined, with the POD method the solution tends to superimpose the solutions coming from the nearest infarction points used in the POD basis construction and to create an infarction area which is the union of these, so the radius of the infarction that we simulate is larger than the one that we are imposing ($r = 2$).

To compensate for this problem, we decide to use a smaller radius in the case of POD model application: it is sufficient to look at the transmembrane potential to notice that the infarction areas of the solution obtained are more similar to those we previously obtained without using POD (respectively
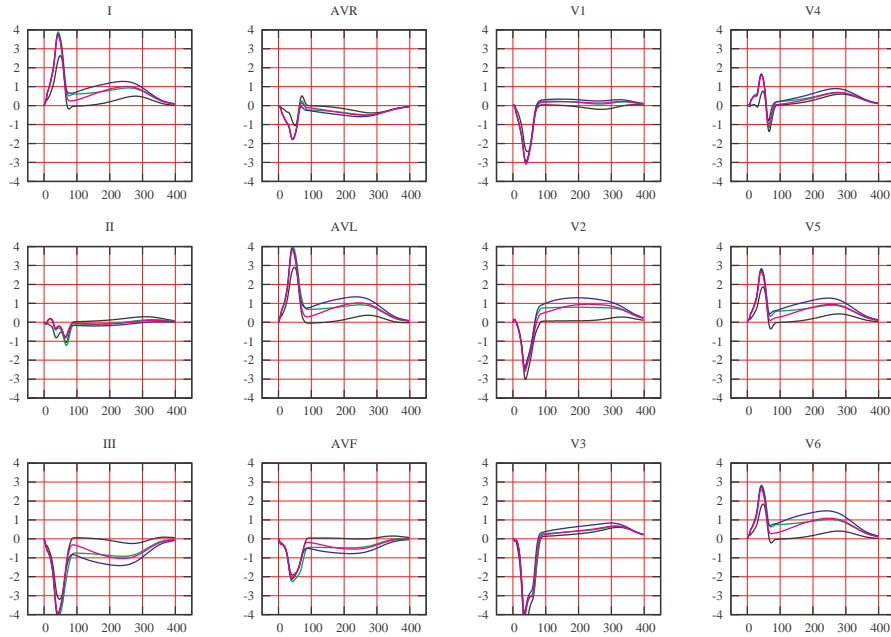
Figure 5.4: Simulated ECG for an infarction centered in point $w =$ $(2.09143, 3.24679, -1.55201)$ not considered in the POD basis: in black the healthy case ECG, in green the ECG obtained modifying the $\tau_{out}$ with the complete model and a radius $r = 2$, in blue the ECG obtained using POD model (always modifying $\tau_{out}$) with the same radius $r = 2$ and in pink the one obtained using POD and a smaller radius $r = 1.5$.

right columns and top images of Figure 5.5). Finally, if we compare the resulting ECG (pink line, Figure 5.4) with the complete model one, we notice that the two solutions are not exactly superimposed as in the "point a" case (which is used to build the basis), but the curves are closer than in the case of equal radius. Anyhow, we can see that trend and magnitude are the same and we have a good approximation of the curve, even if the section between the QRS complex and the ST segment is still difficult to detect.

We remark that using a smaller radius for POD is not totally satisfactory. It is nevertheless conjectured that this would be unnecessary with a larger number of precomputed infarcted regions. In fact, simulating an infarction in a region closer to one of precomputed points conducts to better results without manipulating the radius in the reduced problem. Of course, using a POD basis built with a large number of solutions requires a bigger matrix hardly supported by usual computers memory.

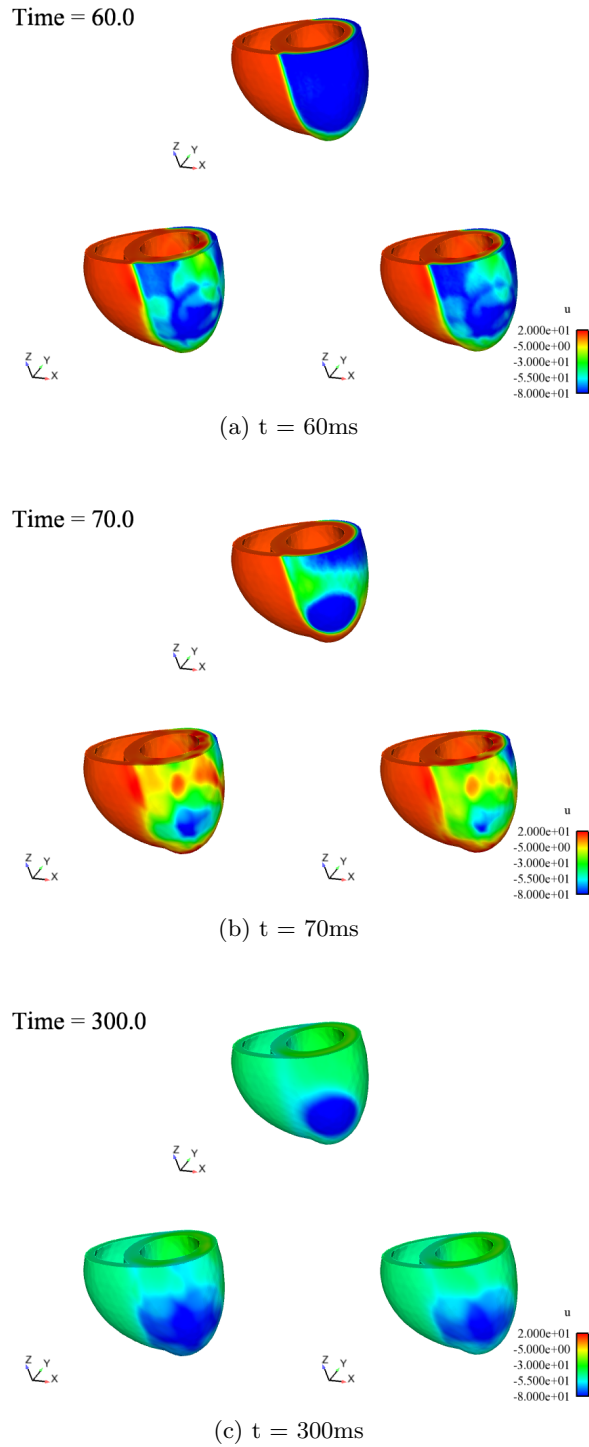This will be investigated in future works.

(a) t = 60ms



(b) t = 70ms



(c) t = 300ms

Figure 5.5: Infarction in point $w = (2.09143, 3.24679, -1.55201)$ generated by modifying the $\tau_{\text{out}}$ constants, using the complete model on the left and the POD method on the right and a reduced infarction ray.

## 5.3 Inverse problem

The most interesting application presented here is the resolution of the inverse problem: we want to identify few parameters of the model looking at the ECG. Particularly, in this case, we are looking for the infarction center. The reference ECG is synthetic, obtained by simulating an infarction centered in a given point with a complete model resolution. This problem has not yet been studied deeply because of the high computational costs of the resolution of the direct problem. We can however mention that different techniques have been explored, see for instance [14]. Our approach is the closest to the medical practice, in the sense that we look directly at the ECG results to keep information on the ischemia.

The procedure used to solve the inverse problem is based on the approximated genetic algorithm described in chapter 3. At each iteration of the genetic algorithm, the exact evaluations of the objective function are computed with a reduced order approximation of the direct problem (in this case based on the POD). The use of reduced order approach makes this technique reasonable in terms of computational time. The cost function is the difference in the ECG as previously described. This criteria can be improved giving for instance more weight to the ST deviation, as suggested in [9].

If we refer to the optimization problem previously described:

$$j^* = \arg \min_{j \in I} \Psi(j),$$

where

$$\Psi(j) = \delta t \sum_{i=1}^{N_t} \left( |\mathrm{I}^{(j)}(t_i) - \mathrm{I}^{(\mathrm{ref})}(t_i)|^2 + |\mathrm{II}^{(j)}(t_i) - \mathrm{II}^{(\mathrm{ref})}(t_i)|^2 + \ldots \right.$$

$$\left. \ldots + |V_6^{(j)}(t_i) - V_6^{(\mathrm{ref})}(t_i)|^2 \right),$$

it remains to identify the subset $I \subset \mathbb{R}^3$. As we said before, the infarction center is localized on the epicardium of the left ventricle so we look for a subset $I$ such that $I \subset \{(x, y, z) \in \delta\Omega_{\mathrm{H}}\}$. If we look at the geometry of the left ventricle we can notice that it is an ellipsoid of the type $\{(x, y, z) \mathrm{s.t.} \frac{x^2}{\alpha^2} + \frac{y^2}{\alpha^2} + \frac{z^2}{\beta^2} = 1\}$, where $\alpha = R_{max} = 4$, $\beta = 7.2$. It is truncated by an $xy$ plane and we also consider a truncation by an $yz$ plane ($x = 0$) to be on the external surface of the heart. The $x$ coordinate of this geometry varies between the values $a = 0$ and $b = R_{max} = 4$, while its $y$ coordinate variates between the values $c$ and $d$ depending on $x$: $c = c(x) = -\sqrt{R_{max}^2 - x^2}$, $d = d(x) = +\sqrt{R_{max}^2 - x^2}$. Finally, for each $xy$ plane we can find two corresponding $z$ coordinates: $z = z(x, y) = \pm\beta\sqrt{1 - \frac{x^2+y^2}{\alpha^2}}$.

---

**Algorithm 4** Approximated Genetic Algorithm

Choice an initial population $P_1 \subset I$ s.t. $\forall x \in P_0, x_i \in [x^i_{\min}, x^i_{\max}]$
$n_g = 1$
**while** $n_g < N_g$ **do**
  **if** $n_g < N_{\text{exact}}$ **then**
    exact evaluation of $\Psi(x) \;\forall x \in P_{n_g}$
  **else**
    approximated evaluation of $\Psi(x) \;\forall x \in P_{n_g}$
    exact evaluation of $\Psi(x)$ for the best $rn_g \; x \in P_{n_g}$
  **end if**
  $m = \min_{x \in P_{n_g}} \Psi(x)$
  $X_{n_g} = \arg\min_{x \in P_{n_g}} \Psi(x)$
  **elitism** :
  **if** $n_g > 2$ and $J(X_{n_g - 1}) < m$ **then**
    $x^i_{n_g} = X_{n_g}$ for a random $i$
  **end if**
  **for** k from 1 to $N_{\text{p}}/2$ **do**
    **selection** of $(x^\alpha_{n_g}, x^\beta_{n_g})$
    replace $(x^\alpha_{n_g}, x^\beta_{n_g})$ with $(y^\alpha_{n_g}, y^\beta_{n_g})$ by **crossover**
    replace $(y^\alpha_{n_g}, y^\beta_{n_g})$ with $(z^\alpha_{n_g}, z^\beta_{n_g})$ by **mutation**
  **end for**
  $n_g = n_g + 1$
  $P_{n_g} = P_{n_g} \bigcup X_{\text{new}}$
**end while**
**return** $X = \arg\min_{x \in P_{N_g}} \Psi(x)$

---

Figure 5.6: The mesh and the 18 points used to build the POD basis. The point out of the mesh lines, indicated by the pink arrow, is the ones we try to find.

Once the minimization function and the subset of the feasible solutions are defined, we can apply the genetic algorithm with approximated evaluations as described in chapter 3 (Algorithm 4).

Now we apply the algorithm to find the point of coordinates $w = (1.53154, -3.34528, -2.70672)$ that has not been used to build the POD basis: the center of the infarction is indicated in Figure 5.6 with an arrow, while the others points are those used to build the POD basis. The reference ECG is obtained solving the complete model for the point $P$ infarction problem. The genetic algorithm is run with $N_p = 80$, $N_g = 15$ and $N_{ex} = 600$, and the parameters we estimate are $\theta = (x_P, y_P, z_P) \in I$.

The solution given by the algorithm is the point of coordinates $\widetilde{w} = (1.12260, -3.64059, -2.19413)$. The corresponding results are exposed in Figures 5.7 and 5.8. We notice that the reference ECG (blue line in Figure 5.7) is well approximated by the one obtained from the resolution of the genetic algorithm (blue line) that leads to find an infarcted center (right column of Figure 5.8) very close to the reference one (right column).
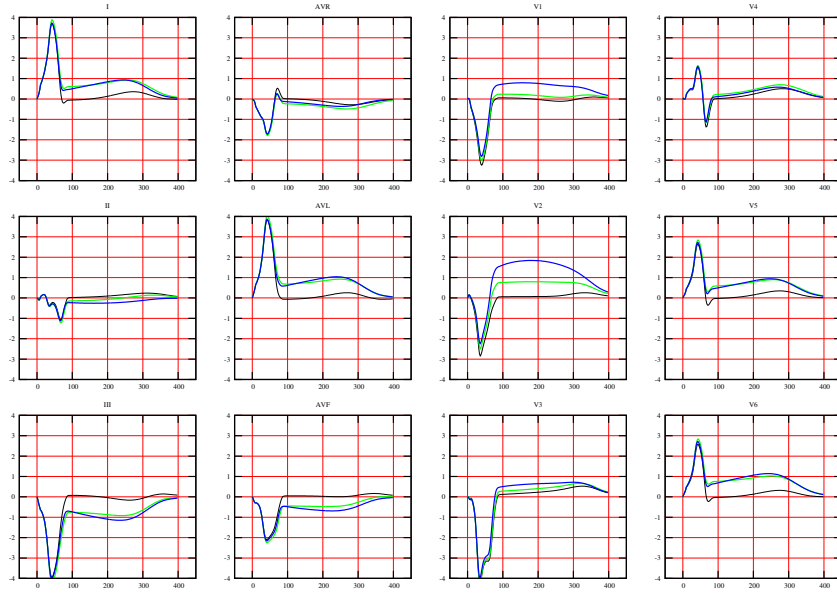
Figure 5.7: Simulated ECG for an infarction located in point $w$: green line represents the simulated reference ECG and blue line the ECG corresponding to the infarcted center found with the resolution of a genetic algorithm. Black line gives the healthy reference case.
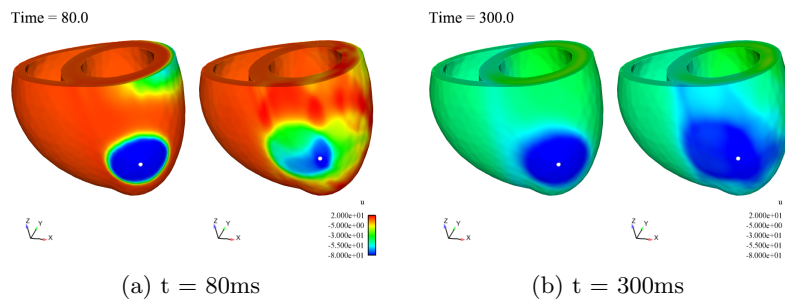


(a) t = 80ms                    (b) t = 300ms

Figure 5.8: On the left column the transmembrane potential calculated in the reference case solved with the complete model, on the right column the transmembrane potential of the solution found with the genetic algorithm obtained with the POD. The white dots indicate the center of the infarcted areas.

# Part III

# The restitution curve

# Chapter 6

# Electrophysiology for a single cell

The second application of the models seen in this work is the study of characteristic times of diastole and systole phases, i.e. the time of relaxations and contractions of the cardiac muscle. This two period have a strong link with the depolarization and repolarization phases described by the electrical model.

Even for a singular cell it is useful to study the so-called restitution curve, that is the relationship between the time of depolarization and the time of repolarization of the previous beat. To study this relationship we need to simulate a long sequence of accelerated beats, about one hundred. The computational time to make these simulations is very long, that is why we first study and test the theory results on a simplified model. Particularly, before dealing with the 3D simulation of the heart, we first look at a 0D model of a single cell, at the trend of the ionic model used to describe it and at the characteristics of its depolarization and polarization phases.

## 6.1   The ionic model

We consider a single cell, as in chapter 1 we still want to determine the transmembrane potential of the cell, i.e. the difference between the potential in the intra and the extra-cellular tissue, $v = u_{\mathrm{i}} - u_{\mathrm{e}}$. In the case of a single cell it is sufficient to consider the ionic model described before. Equation (1.2) can be simply written as an ordinary differential equation:

$$\frac{\partial v}{\partial t} + I_{\mathrm{ion}} + i_{\mathrm{app}} = 0,$$

where the variable are dimensionless, and we only need a description of the ionic current to close the model. In particular, if we consider $i_{\mathrm{app}} = 0$ (not

verified only in the first $2msec$ in which we apply the stimulus), we can say that $\frac{dv}{dt} = -I_{\text{ion}}$.

We consider again the Mitchell and Schaeffer model to describe the ionic current, introduced in section 1.3. The considered functions are the transmembrane potential $v(t)$ and the gating variable $h(t)$, both functions are dimensionless and vary between 0 and 1. The potential $v$ depends on the inward current $J_{in} = \frac{hv^2(1-v)}{\tau_{in}}$ and the outward current $J_{out} = \frac{v}{\tau_{\text{out}}}$,

$$\frac{dv}{dt} = J_{in} - J_{out},$$

where the parameters $\tau_{\text{in}}$ and $\tau_{\text{out}}$ are time constants. The gate variable $h$ describes the opening and closing of the ionic channel gate (i.e. it is equal to 1 when the gate is open and equal to 0 when it is closed). Also the behavior of $h$ depends on two parameters, $\tau_{\text{open}}$ and $\tau_{\text{close}}$, that regulate the opening and closing phases. The ODE system that governs the model is:

$$
\begin{aligned}
\frac{dv}{dt} &= \frac{hv^2(1-v)}{\tau_{\text{in}}} - \frac{v}{\tau_{\text{out}}} \\[2mm]
\frac{dh}{dt} &= \begin{cases} \dfrac{1-h}{\tau_{\text{open}}} & , \quad v < v_g \\[3mm] \dfrac{-h}{\tau_{\text{close}}} & , \quad v > v_g, \end{cases}
\end{aligned}
\tag{6.1}
$$

where $v_g$ is the change-over voltage. So, the system of ODE (6.1) it is sufficient to describe the model of a single cell.

## 6.2 Response to a single stimulus

Mitchell and Schaeffer, in [12] show the solution of their ionic model and conduct a study of the asymptotic times of depolarization and repolarization phases. We want to reproduce results of [12], neglecting the condition imposed in their paper

$$\tau_{\text{in}} \ll \tau_{\text{out}} \ll \tau_{\text{open}}, \tau_{\text{close}}. \tag{6.2}$$

In their paper this assumption is the basis of most of the relations they find out, even if they point out that it doesn't hold for all physiological models. Moreover, in the 3D simulation, this assumption is not satisfied.

If we suppose to start with a rest state, it corresponds to point $(v, h) = (0, 1)$ at initial time. As described in section 1.1.1 the cell electrical cycle is divided into four phases. First, as the gate is open ($h = 1$), it lets enter into the cell the sodium $Na$: there is an inward ionic current ($I_{\text{ion}} < 0$) so $v$ increases quickly to 1, i.e. the cell is depolarized, with the characteristic time $\tau_{\text{in}}$ while the change in $h$ in this period is negligible. Then the gate
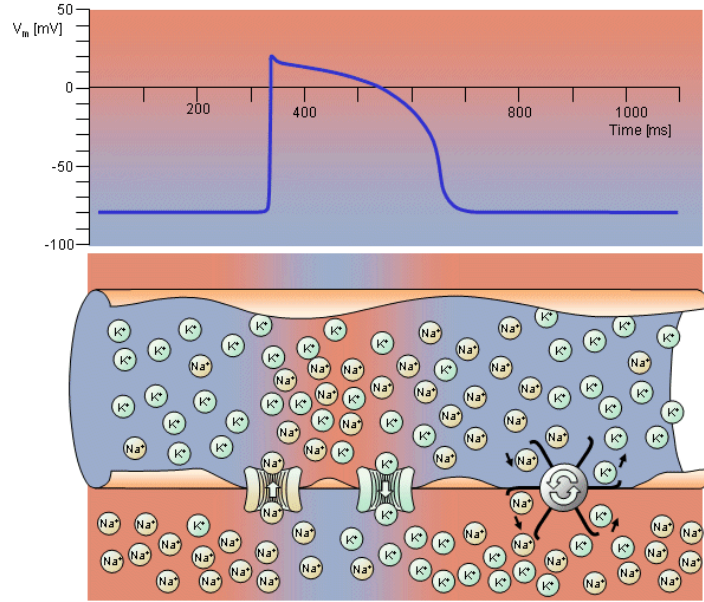
Figure 6.1: Electrophysiology of the cardiac muscle cell (Source: bembook [10]). We can see the two main kind of ions transportation, ionic channels and pumps, and the transmembrane potential $V_m$ during a complete cycle.

closes, i.e. $h$ decreases from 1 to its minimal value $h_{min}$, and we have the phase of *plateau*: the ionic current is negligible, that implies that $v$ stays for a time of order $\tau_{\text{close}}$ almost constant. The polarization phase follows the plateau: the pump creates an outward ionic current $(I_{\text{ion}} > 0)$[1], so $v$ decreases rapidly during a time scale of order $\tau_{\text{out}}$ and the ionic channel is still closed $(h(t) \simeq h_{min})$. Finally, during the fourth phase the ions tends to go back to rest: the $Na$ gate opens that implies $h(t) \simeq 1$, the inward current caused by the sodium is balanced with the outward current of the calcium, so $I_{\text{ion}} \simeq 0$ and $v$ is constant.

Particularly, if the time[2]

$$t^* \text{ such that } v(t^*) = v_g \tag{6.3}$$

is known, we can determine the minimal value risen by the gate variable $h$ during the plateau, $h(t^*) = h_{min}$, because of the solution of the second equation of (6.1) is an exponential:

$$h(t) = \begin{cases} e^{-t/\tau_{\text{close}}} & , t < t^* \\ 1 - (1 - h_{min})e^{-(t-t^*)/\tau_{\text{open}}} & , t > t^* \end{cases} \tag{6.4}$$

---

[1]We remind that pump lets into the cell 2 ions of potassium $K^+$ and lets out 3 ions of sodium $Na^+$.

[2]We suppose the time such that $v < v_g$ at the beginning of the simulation to be negligible.

If we simulate an impulse of period $1.1 sec$ in a single cell, with and without the assumption (6.2) we find the results illustrated in Figures 6.2 and 6.3: ionic parameters take values showed in Table 6.1[3]. In Figure 6.2 we see that $v$ and $h$ follow the trend described above and that the minimal value of $h$ is reached at the time $t^*$ such that $v(t^*) = v_g$. In Figure 6.3 we see the relationship between $h$ and $v$ for different values of ionic parameters and notice that the difference between the minimal values of $h$ is important.

| $\tau_{in}^A$ | $\tau_{out}^A$ | $\tau_{in}$ | $\tau_{out}$ | $\tau_{open}$ | $\tau_{close}$ | $v_g$ |
|---|---|---|---|---|---|---|
| 0.08 | 1.8 | 1.6 | 36 | 100 | 300 | 0.13 |

Table 6.1: Ionic parameters, $\tau_{in}^A$ and $\tau_{out}^A$ correspond to the case when (6.2) is true while $\tau_{in}$ and $\tau_{out}$ to the the case when (6.2) is not satisfied.

To find out an analytical expression of $h_{min}$ which depends on the ionic parameters, Mitchell and Schaeffer suppose that the solution $(v, h)$ is on the nullcline of the first equation of (6.1) (see Figure 6.3) thus it satisfies equation

$$0 = \frac{hv^2(1-v)}{\tau_{in}} - \frac{-v}{\tau_{out}},$$

so the relation between $h$ and $v$ is:

$$h = \frac{\tau_{in}}{\tau_{out}} \frac{1}{v(1-v)}$$

and the minimal feasible value for $h$ is:

$$\widetilde{h} = 4\frac{\tau_{in}}{\tau_{out}}. \tag{6.5}$$

If we go back to Figure 6.3 we can see that the minimum of $h$ corresponding to the green line (assumption (6.2) true) is close to the approximated one, while the minimum of the blue one (assumption (6.2) false) is smaller. We can justify this difference looking at the four different phases: the main condition that has to be respected to correctly evaluate the minimum value of $h$ is $\tau_{out} \ll \tau_{open}$, i.e. the third phase should be negligible compared to the last one. So if we take a smaller $\tau_{out}$ this phase is quicker and $h$ stays close to the approximated value.

---

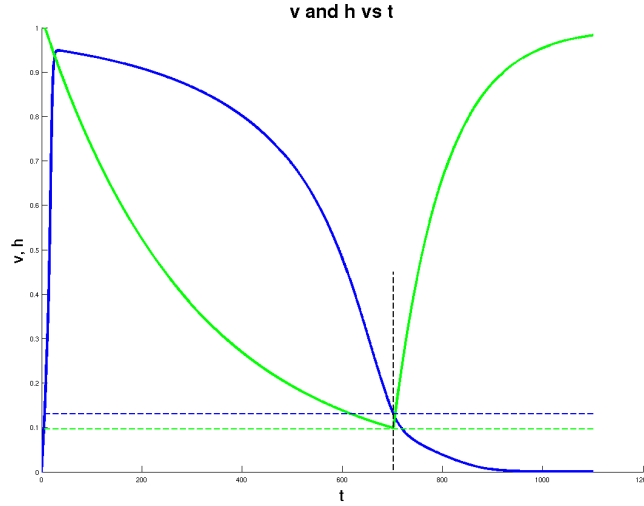[3]We remember that here we are considering a dimensionless model.

Figure 6.2: Gating variable $h$ (green line) and voltage trace $v$ (blue line) as functions of time when the asymptotic condition (6.2) is violated. Horizontal lines indicate the values of $h$ and $v$ at the changeover time $t^*$ defined in (6.3).
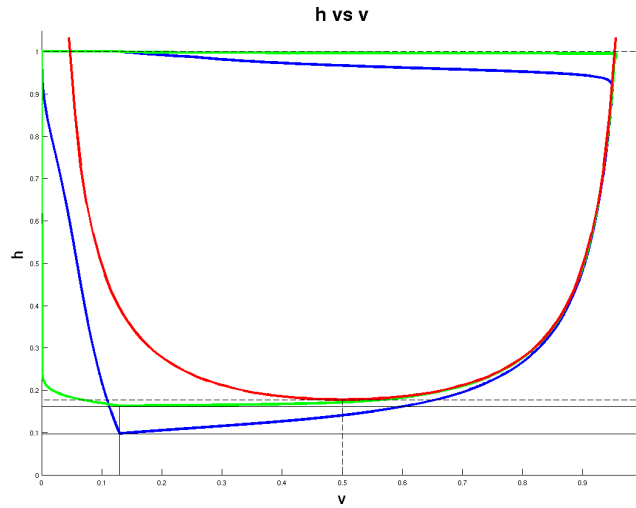


Figure 6.3: Nullcline (red line) and trajectory of $(h, v)$ for different $\tau_{\text{in}}$ and $\tau_{\text{out}}$ values: under hypothesis (6.2) (green line) we have taken $\tau_{\text{in}} = 0.08$, $\tau_{\text{out}} = 1.8$; the case when this condition does not hold (blue line) corresponds to $\tau_{\text{in}} = 1.6$, $\tau_{\text{out}} = 36$; $\tau_{\text{open}}$ is always 100 and $\tau_{\text{close}}$ is 300. Horizontal lines indicate respectively (from top to bottom) the approximated value $\widetilde{h}$ of $h_{min}$ defined in (6.5), the real value of $h_{min}$ under hypothesis (6.2) and the real value of $h_{min}$ when hypothesis doesn't hold.

## 6.3  Multiple stimuli

Our aim is now to find a relationship between the diastolic and the systolic time, i.e. the time of depolarization and polarization of the cell. To do so we obviously have to study a (long) sequence of beats of different period: we will consider a sequence of 60 accelerated beats, the first one of period $1.1sec$ and the next ones decreasing of $10msec$ at each beat.

According to Mitchell and Schaeffer [12], we define the action potential duration (APD) as the time during which the voltage is greater than $v_g$, and $DI$ the time during which $v$ is smaller than (or equal to) $v_g$. Mitchell and Schaeffer say that for multiple stimuli, under assumption $\tau_{\text{in}} \ll \tau_{\text{out}} \ll \tau_{\text{open}}, \tau_{\text{close}}$ i.e. $h_{min} \simeq \widetilde{h}$, the APD of the $(n+1)^{th}$ stimulus depends on the DI of the $n^{th}$ one according to equation:

$$APD(DI) = \tau_{\text{close}} \ln \Big( \frac{1 - (1 - h_{min})e^{-DI/\tau_{\text{open}}}}{h_{min}} \Big). \qquad (6.6)$$

The first observation is that if we replace $t^*$ defined in (6.3) with $APD$ in equation (6.4) we find:

$$h(t) = \begin{cases} e^{-t/\tau_{\text{close}}} & , t \leq APD_1 \\ 1 - (1 - h_{min})e^{-(t-APD_1)/\tau_{\text{open}}} & , APD_1 < t \leq APD_1 + DI_1. \end{cases}$$

More in general it is easy to find the exact solution of the second equation of (6.1). If we define

$$t_{2k} = \sum_{i=1}^{k-1}(APD_i + DI_i), \ t_{2k+1} = \sum_{i=1}^{k-1}(APD_i + DI_i) + APD_k, \ k = 0, 1, 2, \ldots,$$

where $APD_i$ and $DI_i$ indicate respectively the action potential duration and the diastolic time of the $i^{th}$ beat, we know that $h(t_{2k+1}) = h_{min}$, $k = 0, 1, 2, \ldots$. So for all $k = 0, 1, 2, \ldots$

$$h(t) = \begin{cases} h(t_{2k})e^{-(t-t_{2k})/\tau_{\text{close}}}, & t_{2k} < t \leq t_{2k+1} \\ 1 - (1 - h_{min})e^{-(t-t_{2k+1})/\tau_{\text{open}}}, & t_{2k+1} < t \leq t_{2k+2}, \end{cases}$$

with $h(t_0) = 1$ and for $k \geqslant 1$

$$h(t_{2k}) = 1 - (1 - h_{min})e^{-(t_{2k}-t_{2k-1})/\tau_{\text{open}}} = 1 - (1 - h_{min})e^{-DI_{k-1}/\tau_{\text{open}}}.$$

Considering the $k^{th}$ beat and rescaling for $t \in (0, APD_k + DI_k)$ we find

$$h^{(k)}(t) = \begin{cases} h_0^{(k)}e^{-t/\tau_{\text{close}}}, & 0 < t \leq APD_k \\ 1 - (1 - h_{min})e^{-(t-APD_k)/\tau_{\text{open}}}, & APD_k < t \leq APD_k + DI_k, \end{cases}$$

where

$$h_0^{(k)} = 1 - (1 - h_{min})e^{-DI_{k-1}/\tau_{\text{open}}}$$
$$h^{(k)}(APD_k) = h_{min} = h_0^{(k)}e^{-APD_k/\tau_{\text{close}}}, \ k \geqslant 2.$$

Finally we have

$$h_{min} = \left(1 - (1 - h_{min})e^{-DI_{k-1}/\tau_{\text{open}}}\right)e^{-APD_k/\tau_{\text{close}}}$$

that leads to

$$APD_k = \tau_{\text{close}} \ln\left(\frac{1 - (1 - h_{min})e^{-DI_{k-1}/\tau_{\text{open}}}}{h_{min}}\right), \ k = 1, 2, \ldots.$$

So we can conclude that the relationship between $APD_{k+1}$ and $DI_k$ is exact and holds even when assumption $\tau_{\text{in}} \ll \tau_{\text{out}} \ll \tau_{\text{open}}, \tau_{\text{close}}$ is not respected.

If we are not under assumption (6.2) and we assume that $h_{min}$ is given by $\widetilde{h} = 4\frac{\tau_{\text{in}}}{\tau_{\text{out}}}$, we can see in Figure 6.4 that there is a gap of about $100msec$ between the analytic curve (green line) and the curve obtained with simulation (red crosses), while if we use the analytic expression of $h_{min}$ that we can find out looking at the first beat:

$$h_{min} = e^{-APD_1/\tau_{\text{close}}} = e^{-APD_{max}/\tau_{\text{close}}}, \tag{6.7}$$

we find a curve (blue line in Figure 6.4) perfectly superimposed to the experimental one.

Finally, we point out that $APD_{max}$ is the asymptotic value of the so-called restitution curve $APD(DI)$. In fact, if we substitute the value of $h_{min}$ we find:

$$APD(DI) = \tau_{\text{close}} \ln\left(\frac{1 - (1 - e^{-APD_{max}/\tau_{\text{close}}})e^{-DI/\tau_{\text{open}}}}{e^{-APD_{max}/\tau_{\text{close}}}}\right) =$$

$$= APD_{max} + \tau_{\text{close}} \ln\left(1 - (1 - e^{-APD_{max}/\tau_{\text{close}}})e^{-DI/\tau_{\text{open}}}\right), \tag{6.8}$$

so it's easy to verify that

$$\lim_{DI\to\infty} APD(DI) = APD_{max}.$$

## Conclusions

It is shown in [12] that the relationship 6.6 holds with $h_{min} = 4\frac{\tau_{\text{in}}}{\tau_{\text{out}}}$ under the restrictive assumption $\tau_{\text{in}} \ll \tau_{\text{out}} \ll \tau_{\text{open}}, \tau_{\text{close}}$. We have shown here that the formula is in fact valid without restrictions if we define $h_min$ by (6.7). Nevertheless, this expression of $APD(DI)$ is easier to calculate as it depends only on the two ionic parameters $\tau_{\text{open}}$ and $\tau_{\text{close}}$ and on the value of $APD_{max}$. We finally remark that the value of $APD_{max}$ can be simply find looking at the asymptotic value of an experimental restitution curve or simulating two long beats (corresponding to a very low frequency as for instance 40 or 50 beats per minute).
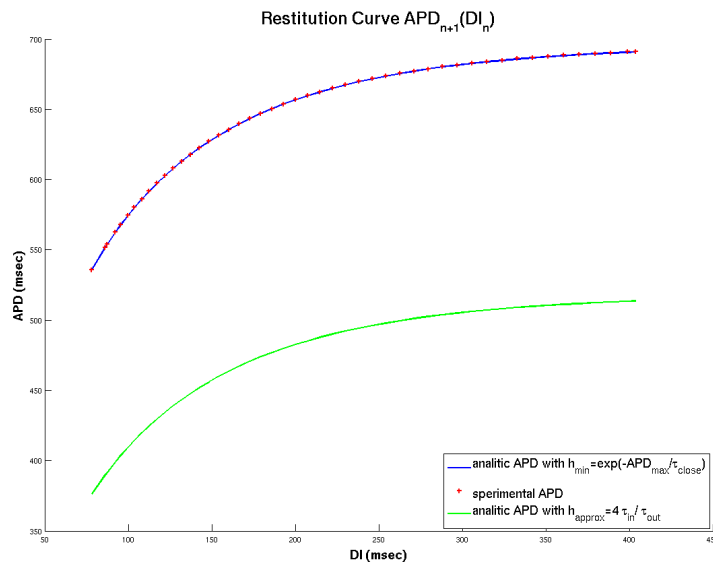
Figure 6.4: Red crosses represent the restitution curve obtained with 60 stimuli, the first one of period $1sec$, and decreasing of $10msec$ each iteration. Blue line is the analytic function of APD(DI) with the real value of $h_{min}$ and the green one with the approximated one.

## 6.4 Parameters identification

Now that the model is well defined and that we have verified that the analytic value of the restitution curve

$$APD(DI) = APD_{max} + \tau_{\text{close}} \ln\left(1 - (1 - e^{-APD_{max}/\tau_{\text{close}}})e^{-DI/\tau_{\text{open}}}\right),$$

holds without any additional hypothesis we would like to use this information to estimate the parameters of the model. The idea is to compare the simulated curve and an analytic one and to minimize the difference between them with respect to the ionic parameters. It is clear that we expect to estimate only three parameters: $\tau_{\text{open}}$, $\tau_{\text{close}}$ and $APD_{max}$. The $\tau_{\text{in}}$ and $\tau_{\text{out}}$ are strictly linked to the variation of $v$ and they are lie into the model.

Referring to [11], we use a non linear least squared method to minimize the error between the simulated values $APD_n$ and the analytical ones $APD(DI_n, \theta)$:

$$\min_{\theta} \sum_{n=1}^{N} (APD(DI_n, \theta) - APD_{n+1})^2,$$

where $\theta = (\tau_{\text{open}}, \tau_{\text{close}}, APD_{max})$. Particularly, we used the software $R$ to calculate these parameters. Here are the command of the *Nonlinear least square regression* (NLS) described in [6]:

```
> f<-function(DI,tau_open,tau_close,APDmax){
  APDmax+
  tau_close*log(1-(1-exp(-APDmax/tau_close))*exp(-DI/tau_open))
  }
>
> NLS<-nls(APD~f(DI,tau_open,tau_close,APDmax),
  start=c(tau_open=150,tau_close=150,APDmax=1100))
>
> summary(NLS)

  Formula: APD ~ f(DI, tau_open, tau_close, APDmax)

  Parameters:
            Estimate Std. Error t value Pr(>|t|)
  tau_open  100.01538    0.04478    2234   <2e-16 ***
  tau_close 300.19651    0.21092    1423   <2e-16 ***
  APDmax    695.92985    0.01475   47180   <2e-16 ***
  ---
  Signif. codes:  0 *** 0.001 ** 0.01 * 0.05 . 0.1   1

  Residual standard error: 0.02868 on 44 degrees of freedom
```

```
Number of iterations to convergence: 6
Achieved convergence tolerance: 8.537e-07
```

It requires the sample to be fitted (APD,DI), the analytical expression of the curve and an initial point $\theta_0$. We impose the analytical expression of $f(DI) = APD(DI)$ as described above and we choose a feasible initial value supposed to be a feasible solution, $\theta_0 = (150, 150, 1100)$.

As the sample is calculated artificially we know that the exact solution is $\theta^* = (100, 300, 691.1)$ while looking at the $R$ output we find that the estimated solution is $\theta = (100.01538, 300.1965, 695.92985)$, which is very close to the exact one. We can also look at the second and third columns of the $R$ output: the `Std. Error` indicates the standard deviation of the estimated parameter and the `t value` the inverse of the relative confidence interval length, i.e. the ratio between the first and the second columns. We can observe that the standard error is small and that the `t value` is more than $10^3$ for all the parameters that means that our solution is estimated with a tiny incertitude.

Finally we plot the simulated values of APD and DI (blue points) and the analytical curve obtained with the estimated parameters (red line) in Figure 6.5: we verify that the two curves are completely superimposed, i.e. the estimated values perfectly fit the used ones.
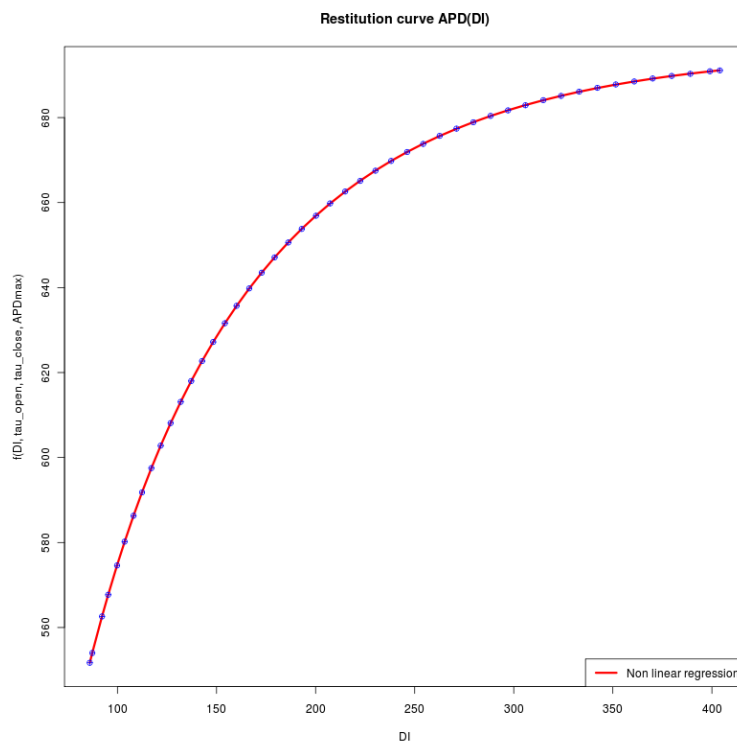
Figure 6.5:  Blue points represent the restitution curve obtained with 60 stimuli, the first one of period $1sec$, and decreasing of $10msec$ each iteration. Red line is the analytic function of APD(DI) obtained substituting the estimated parameters.

# Chapter 7

# ECG-based restitution curve

The previous chapter shows how to estimate some parameters of the ionic model using only the so-called restitution curve obtained from a 0D model for one cell. In this chapter we try to extend these results to a 3D model of the heart, using the restitution curve of a single cell belonging to the heart or a restitution curve obtained from an ECG. In the last case, the restitution curve is assumed to give the dependence of the QT time (time between the Q and the T waves) in function of the preceding TQ time, that can be respectively compared with the APD and DI of the single cell. In the complete heart model we have taken four different values for the $\tau_{\text{close}}$ (more details can be found in section 1.3) we decide to impose only one constant value of $\tau_{\text{close}}$, i.e. to use just one type of cells. This assumption leads to a false ECG with inverted T waves, future developments of the problem will probably allow to identify the ionic parameters also in the case of an heterogeneous heart tissue.

## 7.1 POD applications

Long sequences of beats with decreasing periods between each beat allows to construct the so-called restitution curve, i.e. the relationship between the action potential duration (APD) and the diastolic interval (DI) preceding the action potential. This is a medical test which can highlight arrhythmia like fibrillation. As the simulation of a sequence of beats requires a long computational time, we propose to use a POD approach.

Let us consider a long sequence of accelerated beats. In our simulation, the first beat last 1.1s (it corresponds to about 55 beats per minute) and, at each beat, the period decreases of $50ms$. The total simulation lasts $10s$, that leads at the end to a frequency of about 110 beats per second. The normal heart frequency is between 60 and 100 beats per minute. For a frequency greater than about 100 beats per minute we have tachycardia, in our case ventricular tachycardia, and the shape of the ECG becomes unusual.

The simulation is first run with the full order model until the end of the last first beat. Then the POD basis is constructed from this simulation (in particular it is sufficient to keep the first $400ms$ of the solution) and this basis is used for the long-time simulation. Figure 7.1 shows the first lead of the ECGs: we notice that the two solutions are, as expected, perfectly superimposed during the whole simulation.
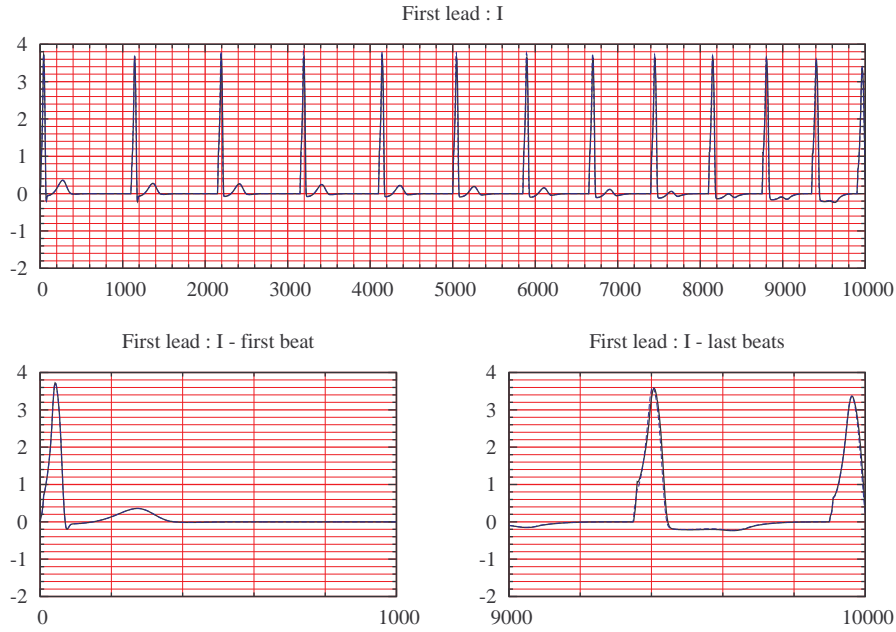


Figure 7.1: Simulated ECG for long period (10 seconds) for accelerated beats (55 beats per minute to 110 beats per minute) with complete model (continuous line) and reduced model (dotted line).

As mentioned before, simulations of realistic ECG have been obtained with an heterogeneous ionic parameter $\tau_{\text{close}}$ in the Mitchell and Schaeffer ionic model (1.9) to obtain a true ECG, in order to have four different kinds of cells depending on the position in the heart domain. A study of the restitution curve based on a real ECG can be subject of future works.

Dealing with the identification of ionic parameters from the restitution curve we can estimate for the moment only one value of $\tau_{\text{close}}$, so we decide to take it constant in the whole heart domain, even if it leads to a wrong ECG: we obtain a negative T wave, opposed to the real one. Results corresponding to this hypothesis are given in Figure 7.2, both with a complete model and a reduced one. In this case too, the POD approach allows to approximate accurately the complete model solution, particularly the two ECG are perfectly superimposed in the first part of the simulation and they present a negligible difference in T wave magnitude during last beats.
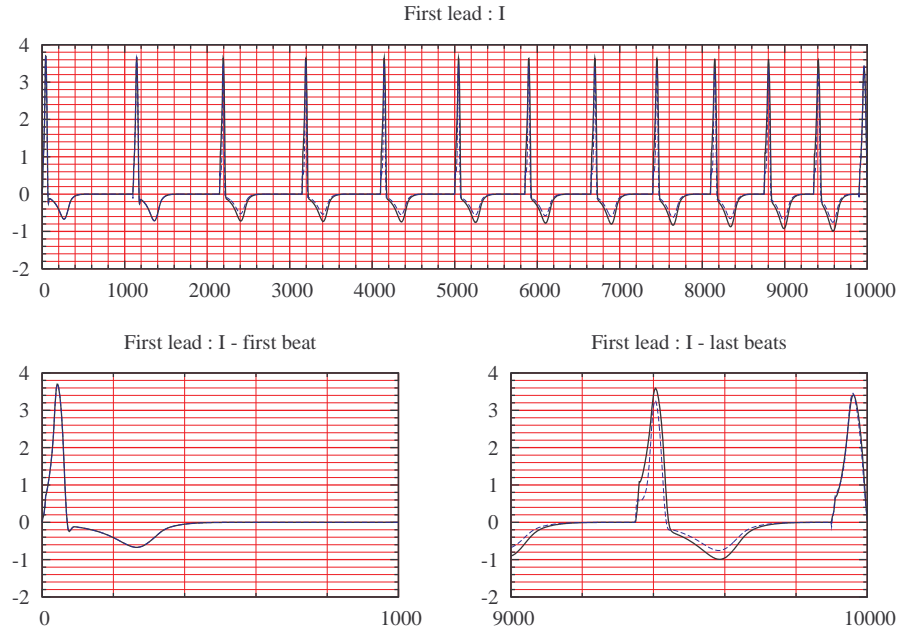
Figure 7.2: Single type cell simulated ECG for long period (10 seconds) for accelerated beats (55 beats per minute to 110 beats per minute) with complete model (continuous line) and reduced model (dotted line).

## 7.2  RC of a single cell of the 3D model

Once verified that the solution obtained with a reduced model well approximates the complete model one, we want to compare the corresponding restitution curves. The first approach is to evaluate the transmembrane potential of a generic single cell and verify if the results of the 0D model exposed in chapter 6 are still valid.

If we look at the restitution curve obtained by recording the transmembrane potential and the corresponding APD and DI times in a cell localized on the epicardium in the right ventricle we find the results showed in Figure 7.3. Let us compare the restitution curve obtained with the solution of the complete model (black curve) and the curve obtained with the reduced one (red curve). We can observe that the two curves are very close. Figure 7.4 shows the same results for a cell localized on the left ventricle. Similar observations can be done, even if the two restitution curves differ more than in the case of the right ventricle cell. We can explain this difference by noticing that the left ventricle is thicker than the right one, so it is more subjected to approximations.

As in chapter 6 we apply again the *Nonlinear least square regression* (NLS) to identify the ionic parameters $\tau_{\text{open}}$ and $\tau_{\text{close}}$ and the maximal
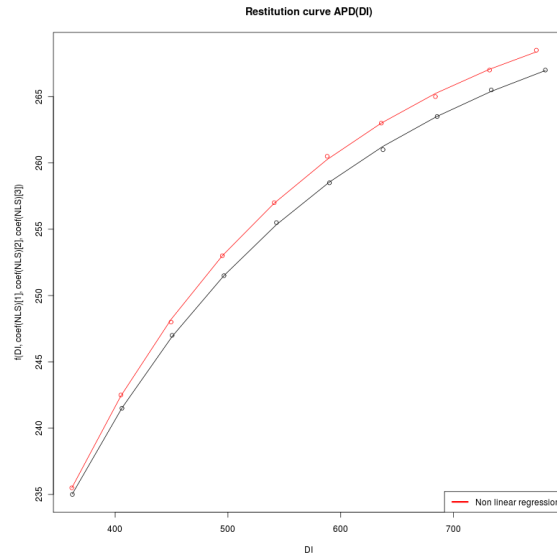
Figure 7.3: Restitution curve of a single cell on the right ventricle, with an homogeneous heart domain, obtained with complete model (black line) and reduced model (red line).
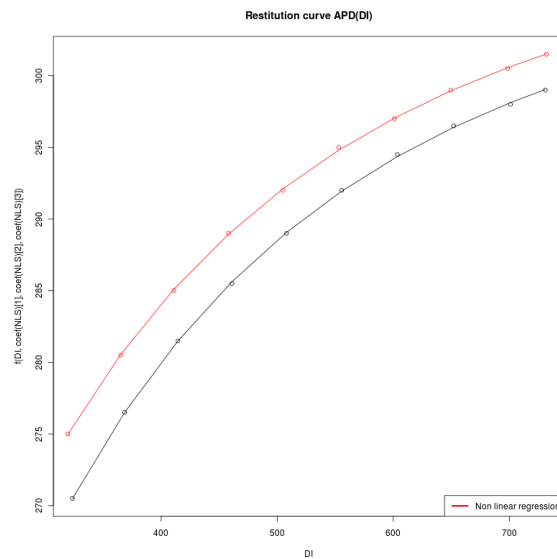


Figure 7.4: Restitution curve of a single cell on the left ventricle, with an homogeneous heart domain, obtained with complete model (black line) and reduced model (red line).

value of APD in these cells. We suppose that the analytical expression of APD(DI) that holds for a single cell model is still valid:

$$APD(DI) = APD_{max} + \tau_{\text{close}} \ln\left(1 - (1 - e^{-APD_{max}/\tau_{\text{close}}})e^{-DI/\tau_{\text{open}}}\right),$$

and we try to approximate the simulated restitution curve with these function. For the left ventricle, using the complete model we obtain results summarized in Table 7.1 while the real parameters are $\tau_{\text{open}} = 300$ and $\tau_{\text{close}} = 100$. In the case of the reduced model results are summarized in Table 7.2

| Parameters | Estimate | Std. Error | t value |
|---|---|---|---|
| $\tau_{\text{open}}$ | 282.9535 | 8.1793 | 34.59 |
| $\tau_{\text{close}}$ | 151.3286 | 8.5411 | 17.72 |
| $APD_{max}$ | 275.1944 | 0.4583 | 600.43 |

Table 7.1: Results obtained with the NLS $R$ algorithm for the curve of Figure 7.3: right ventricle cell with homogeneous heart tissue and complete model. Starting point of the algorithm is $\theta_0 = (200, 150, 300)$. The algorithm converges is 5 iterations and re Residual standard error is 0.1264 on 7 degrees of freedom. The exact solution is $\theta^* = (300, 100, APD_{max})$.

| Parameters | Estimate | Std. Error | t value |
|---|---|---|---|
| $\tau_{\text{open}}$ | 248.052 | 7.878 | 31.48 |
| $\tau_{\text{close}}$ | 219.069 | 20.496 | 10.69 |
| $APD_{max}$ | 275.41 | 0.483 | 570.21 |

Table 7.2: Results obtained with the NLS $R$ algorithm for the curve of Figure 7.3: right ventricle cell with homogeneous heart tissue and reduced model. Starting point of the algorithm is $\theta_0 = (200, 150, 300)$. The algorithm converges is 5 iterations and re Residual standard error is 0.161 on 7 degrees of freedom. The exact solution is $\theta^* = (300, 100, APD_{max})$.

We first notice that the complete model estimation of the parameters is better than the POD one, even if both do not lead to the right value. They converge at the same $APD_{max}$ that is well defined (the t value in both case is more than 550 that means that the Standard Error compared with the mean value is very small, i.e. the parameter is estimated with a tiny incertitude),

but the two ionic parameters are not very close to the real ones. The $\tau_{\text{open}}$ is estimated to be 282.9535 in the case of complete model while is correct value is 300, that implies a relative error of the 5%, while with the reduced model the relative error is 17%. If we look at the $\tau_{\text{close}}$ value we notice that the relative errors with the complete model and with the reduced one are respectively 50% and 175%, i.e. the model can not estimate this parameter at all.

| Parameters | Estimate | Std. Error | t value |
|:---:|:---:|:---:|:---:|
| $\tau_{\text{open}}$ | 308.552 | 8.4535 | 36.5 |
| $\tau_{\text{close}}$ | 89.4160 | 2.7855 | 32.1 |
| $APD_{max}$ | 307.5238 | 0.4004 | 768.1 |

Table 7.3: Results obtained with the NLS $R$ algorithm for the curve of Figure 7.4: left ventricle cell with homogeneous heart tissue and complete model. Starting point of the algorithm is $\theta_0 = (200, 150, 300)$. The algorithm converges is 6 iterations and re Residual standard error is 0.0992 on 7 degrees of freedom. The exact solution is $\theta^* = (300, 100, APD_{max})$.

| Parameters | Estimate | Std. Error | t value |
|:---:|:---:|:---:|:---:|
| $\tau_{\text{open}}$ | 323.4783 | 10.5936 | 30.54 |
| $\tau_{\text{close}}$ | 76.3837 | 2.5343 | 30.14 |
| $APD_{max}$ | 309.7547 | 0.4516 | 685.86 |

Table 7.4: Results obtained with the NLS $R$ algorithm for the curve of Figure 7.4: left ventricle cell with homogeneous heart tissue and reduced model. Starting point of the algorithm is $\theta_0 = (200, 150, 300)$. The algorithm converges is 5 iterations and re Residual standard error is 0.106 on 7 degrees of freedom. The exact solution is $\theta^* = (300, 100, APD_{max})$.

If we look at the cell on the left ventricle considered above, the estimations that we find with the complete model are summarized in Table 7.3 while with the reduced one are summarized in Table 7.4. The solutions $\theta = (308.5529, 89.4160, 307.5238)$ and $\theta_{POD} = (323.4783, 76.3837, 309.7547)$ are much closer to the real ones: the relative errors with the POD approach are 7% in the case of $\tau_{\text{open}}$ and 23% for $\tau_{\text{close}}$. This results leads to the conclusion that results given by the algorithm strongly depend on the chosen

cell, so a good choice of the cell can lead to the right parameters, while for some other cells the results are completely wrong. We can anyway notice that the POD approach leads to results comparable to those obtained with the complete model, both in case of good or bad estimation. So, in future developments of the subject, the POD can be applied.

Finally, we use the "four type of cells" model and we conduct the same studies. We consider a long sequence of beats simulated as in Figure 7.1 and we look at the restitution curve of two different epicardium cells, the first one on the right ventricle and the second one on the left one. The obtained restitution curve are respectively shown in Figures 7.5 and 7.6: we notice again that the results obtained with the reduced model (red curves) are very close to those obtained with the complete one (black ones).

| Parameters | Estimate | Std. Error | t value |
|:---:|:---:|:---:|:---:|
| $\tau_{\text{open}}$ | 264.8388 | 6.3775 | 41.53 |
| $\tau_{\text{close}}$ | 219.9267 | 14.6239 | 15.04 |
| $APD_{max}$ | 277.8336 | 0.4138 | 671.41 |

Table 7.5: Results obtained with the NLS $R$ algorithm for the curve of Figure 7.5: right ventricle cell with heterogeneous heart tissue and complete model. Starting point of the algorithm is $\theta_0 = (200, 150, 300)$. The algorithm converges is 7 iterations and re Residual standard error is 0.1224 on 7 degrees of freedom. The exact solution is $\theta^* = (300, 120, APD_{max})$.

| Parameters | Estimate | Std. Error | t value |
|:---:|:---:|:---:|:---:|
| $\tau_{\text{open}}$ | 268.668 | 15.212 | 17.661 |
| $\tau_{\text{close}}$ | 197.385 | 27.751 | 7.113 |
| $APD_{max}$ | 278.305 | 0.956 | 291.103 |

Table 7.6: Results obtained with the NLS $R$ algorithm for the curve of Figure 7.5: right ventricle cell with heterogeneous heart tissue and reduced model. Starting point of the algorithm is $\theta_0 = (200, 150, 300)$. The algorithm converges is 7 iterations and re Residual standard error is 0.2746 on 7 degrees of freedom. The exact solution is $\theta^* = (300, 120, APD_{max})$.

As we are dealing with single cell restitution curve, even if $\tau_{\text{close}}$ varies from cell to cell, we can try to estimate the ionic parameters locally. If we

investigate the restitution curve of Figure 7.5 for a cell in the right ventricle cell with the same technique used above we obtain for the complete model the values in Table 7.5 and for the reduced one the values in Table 7.6, while the exact solution is $\theta^* = (300, 120, APD_{max})$.

If we consider the left ventricle cell, with the complete model we obtain results in Table 7.7 and with the reduced model the results summarized in Table 7.8 while the exact solution is $\theta^* = (300, 130, APD_{max})$.

| Parameters | Estimate | Std. Error | t value |
|:---:|:---:|:---:|:---:|
| $\tau_{\text{open}}$ | 310.5017 | 9.2177 | 33.69 |
| $\tau_{\text{close}}$ | 109.4269 | 3.2441 | 33.7 |
| $APD_{max}$ | 370.4724 | 0.6276 | 590.3 |

Table 7.7: Results obtained with the NLS $R$ algorithm for the curve of Figure 7.6: left ventricle cell with heterogeneous heart tissue and complete model. Starting point of the algorithm is $\theta_0 = (200, 150, 300)$. The algorithm converges is 5 iterations and re Residual standard error is 0.1481 on 7 degrees of freedom. The exact solution is $\theta^* = (300, 130, APD_{max})$.

| Parameters | Estimate | Std. Error | t value |
|:---:|:---:|:---:|:---:|
| $\tau_{\text{open}}$ | 310.874 | 12.466 | 24.94 |
| $\tau_{\text{close}}$ | 112.482 | 4.681 | 24.03 |
| $APD_{max}$ | 362.380 | 0.847 | 427.82 |

Table 7.8: Results obtained with the NLS $R$ algorithm for the curve of Figure 7.6: left ventricle cell with heterogeneous heart tissue and reduced model. Starting point of the algorithm is $\theta_0 = (200, 150, 300)$. The algorithm converges is 5 iterations and re Residual standard error is 0.1943 on 7 degrees of freedom. The exact solution is $\theta^* = (300, 130, APD_{max})$.

As in the case of homogeneous heart tissue we can conclude that the POD solutions conduct to the same results as the complete model, that allows for future studies to use this "cheaper" approach. Also, as previously observed, the single cell restitution curve does not lead to good results in the parameter estimation as it does not take into account the interactions between cells that modify the single cell cycle intervals.
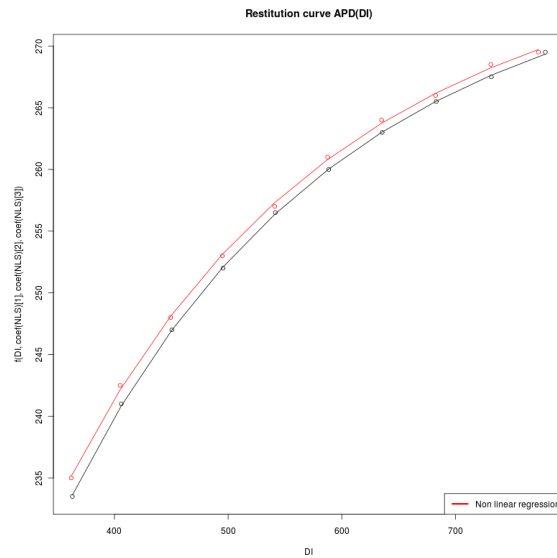
Figure 7.5: Restitution curve of a single cell on the right ventricle, of a "four type of cells" model, obtained with complete model (black line) and reduced model (red line).
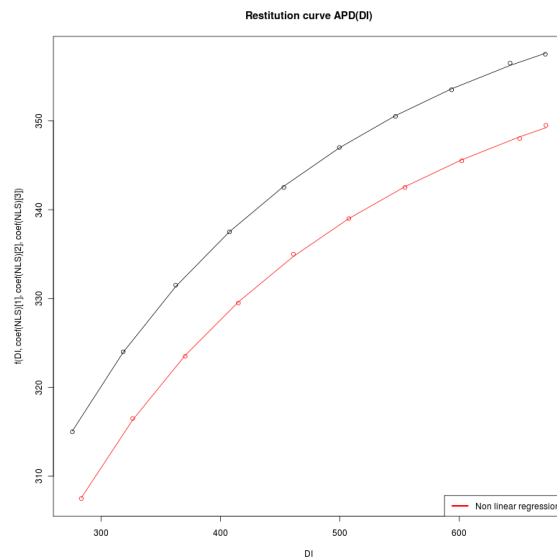


Figure 7.6: Restitution curve of a single cell on the left ventricle, of a "four type of cells" model, obtained with complete model (black line) and reduced model (red line).

## 7.3  ECG-based RC

The next step proposed in this work is to estimate the ionic parameters $\tau_{\text{open}}$ and $\tau_{\text{close}}$ directly from an ECG first lead using the same technique applied for the study of a single cell. This study is based on [11] and it has been conducted with the SYSIPHE team, using their *QT/TQ detection algorithm.*
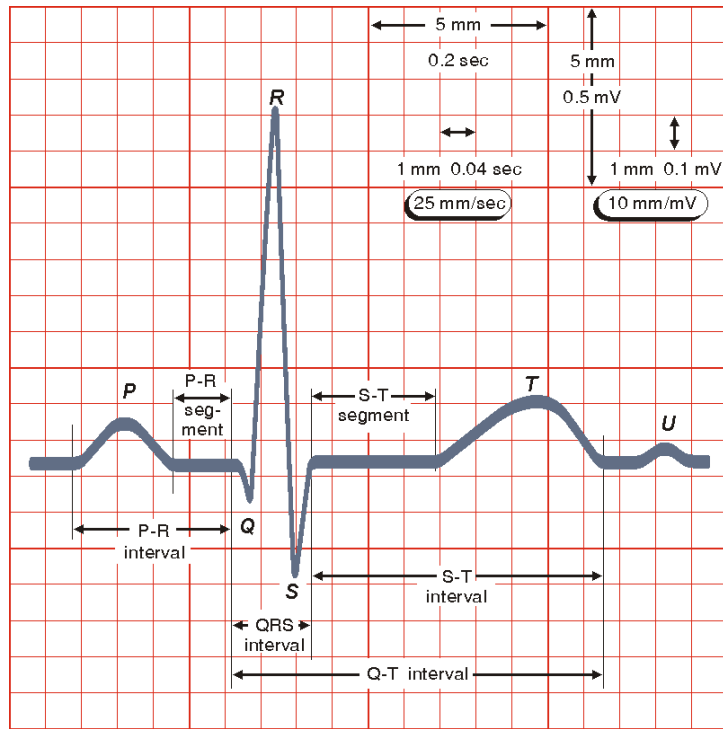


Figure 7.7: The normal electrocardiogram (Source: bembook [10]).

Particularly, [11] explains the relationship between the QT interval and the TQ interval preceding it. The QT interval is the time between the Q and the T waves and represents the systole, i.e. the contraction phase of the heart, while the TQ interval represents the diastole, i.e. the relaxation phase. These two periods can be respectively associated to duration of the ventricular electrical activity and to the next rest period. As the APD represents the depolarization time of a single cell, we can imagine the QT period as the APD of a large number of cells. Therefor, the relationship between the QT and the TQ time is similar to the relationship between the APD and the DI.

The results exposed in [11] show that the restitution curve obtained by plotting the QT interval against the preceding TQ interval has a similar shape compared to the single cell restitution curve APD(DI). We remark

that an essential factor is the use of a good algorithm for the detection of QT and TQ interval, as the one proposed by [11].

Let us consider the simulated long sequence of (realistic) beats shown in Figure 7.1. Using the *T-wave detection algorithm* implemented in [21], we plot the corresponding restitution curve both with the complete and reduced models (Figure 7.8). As the complete and reduced model ECG are superimposed, the restitution curves too are very close. We notice also that on the right of the plot (blue and green curves) the curve trend is completely wrong: we split the curve into two parts. The curves on the left (black and red ones) correspond to the first part of the ECG while the the curves on the right (blue and green ones) are the second part of the simulated ECG. We can say that the left part of the restitution curve is the good one: looking at the ECG in Figure 7.1 we notice that until about 5 seconds the ECG has an usual trend, so the T-wave end algorithm can detect the good QT/TQ intervals. After 5 seconds we see the apparition of a second inverted wave, the detection algorithm does not keep any more the T-wave end but it detects the end of this second wave as the end of the QT interval. This problem leads to a completely wrong restitution curve. Of course, future works can improve the solution of the ionic model in the case of accelerated beats and a more realistic ECG could be obtained. For the time being, the simulated ECG does not lead to an useful restitution curve.
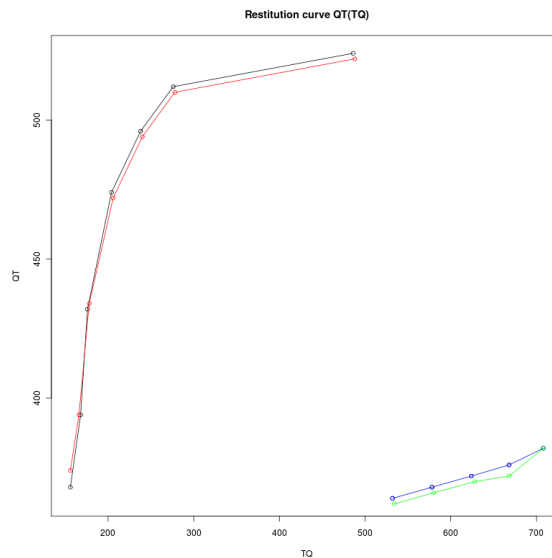


Figure 7.8: Restitution curve obtained from ECG in Figure 7.1 with complete model (black and blue lines) and reduced model (red and green lines). The T-wave detection algorithm given in [21] is used.

The second approach deals with the study of the "one cell" ECG with

inverted T wave: even if the obtained ECG is not realistic the T wave does not present any oscillations, so the T-wave detection algorithm is supposed to find a well defined restitution curve. In order to have a more detailed restitution curve, we consider a longer sequence of beats: 60 beats are simulated, starting from a period of 1.1 seconds and decreasing of $10msec$ each beat (from 50 beats per minute to 120 beats per minute). The results of the QT/TQ ECG-detection are showed in Figure 7.9: blue points are the ECG-based restitution curve and red line is their interpolation.
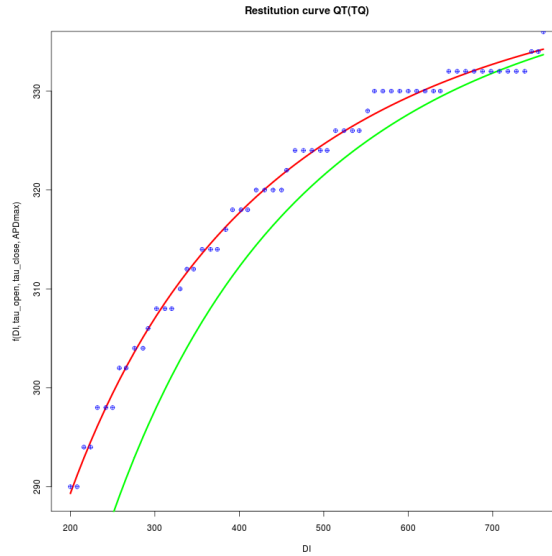


Figure 7.9: Restitution curve obtained from 60 beats ECG (50 to 120 beats per minute) with complete model: blue points represent the numerical values of QT/TQ, red line is their interpolation and green curve is the analytical restitution curve for the real ionic parameters.

As for the one cell case, we apply the *Nonlinear least square regression* (NLS) in order to identify the ionic parameters of the model: we want to verify if the analytical expression of the Action Potential Duration (APD) in function of the Diastolic Interval (DI) that holds for a 0D model can be assumed valid also for a large number of cells represented by a 3D model. The solution of the $R$ algorithm is summarized in Table 7.9. The optimum is $\theta = (343.550, 64.501, 341.674)$ while the exact value is $\theta^* = (300, 100, APD_{max})$. We notice that the points on the curve present a much variability than in the case of the 0D model so the parameters are estimated with a large incertitude (t values less than 20). Also, the relative error of the mean value is 14% for the $\tau_{\text{open}}$ and 35% for the $\tau_{\text{close}}$: the "analytical" and the numerical restitution curves are not perfectly superimposed, but we can observe a similar trend. These preliminary results

obtained with an heterogeneous heart tissue, combined with a better ionic model able to reproduce realistic accelerated beats, can be used for future works concerning a "four cells model".

| Parameters | Estimate | Std. Error | t value |
|:---:|:---:|:---:|:---:|
| $\tau_{\text{open}}$ | 343.550 | 24.477 | 14.04 |
| $\tau_{\text{close}}$ | 64.501 | 3.349 | 19.26 |
| $APD_{max}$ | 341.674 | 1.115 | 306.31 |

Table 7.9: Results obtained with the NLS $R$ algorithm considering the QT/TQ restitution curve (Figure 7.9) obtained from a 60 beats ECG (50 to 120 beats per minute) with complete model. Starting point of the algorithm is $\theta_0 = (200, 150, 300)$. The algorithm converges is 5 iterations and re Residual standard error is 0.9561 on 59 degrees of freedom. The exact solution is $\theta^* = (300, 130, APD_{max})$.

## Conclusions

Restitution curves approach to estimate ionic parameters can be improved and conduct to excellent results. Nevertheless even if we are not yet able to find the parameters with a good approximation we remark that the proposed technique is extremely fast. If we compare it with the genetic algorithms used to find the infarcted area in the precedent part we observe that genetic algorithms lead to a more precise solution but they require a very long computational time. At the state of the art, restitution curves and nonlinear least square regression solution can be used for instance as starting point of an heuristic method as genetic algorithms.

# Conclusions

In this work we have presented two main examples where reduced model and POD approach can be applied in cardiac electrophysiology. Both of them leads to good results and has a useful role in the inverse problem resolution.

The first part deals with the study of the myocardial transmural infarction. We illustrate that it is sufficient to modify one of the ionic parameters of (1.9) to obtain a good simulated infarction and its corresponding ECG. Then, we applied different POD techniques to obtain the solution with a reduced model. We showed that the use of a POD basis generated with an healthy case is not able to reproduce an infarction not included in the POD basis, while a composed POD basis can be used. Particularly, an efficient basis is obtained by collecting snapshots of the solution for multiple located infarctions. This basis can be used to simulate a random point infarction problem with good results.

Then, the inverse problem is explored. We use genetic algorithms to solve a minimization problem and find out the infarcted zone from a simulated ECG obtained with the full model. As genetic algorithms require a lot of resolutions of the problem, POD approach proved to be very useful to decrease the computational time. The resolution of the inverse problem leads to a good approximation of the infarcted area, even with a small number of generations.

The second application concerns the simulation of long sequences of beats. We show that the POD solution can accurately approximate the complete model solution. The use of reduced models leads to much shorter computational time. The simulation of a long sequence of accelerated beats is at the basis of the study of the so-called restitution curve, that is very useful for the detection of arrhythmia. We show that the study of this curve can lead to the identification of some parameters of the ionic model (1.9). Once obtained a realistic ECG, future works could use the simple *Nonlinear least square regression*, as proposed in the present work, to identify the parameters. We remark that this approach is very cheaper in terms of computational cost, while genetic algorithms need the resolutions of the direct problem at each iteration. So restitution curves represent a new approach to be explored in terms of resolution of inverse problems.

# Bibliography

[1] R. Aliev and A. Panlov. *A simple two-variable model of cardiac excitation.* Chaos, Solitons and Fractals, 7(3):293301, 1996.

[2] M. Boulakia, S. Cazeau, M. A. Fernández, J.-F. Gerbeau, N. Zenzemi. *Mathematical Modeling of Electrocardiograms: A Numerical Study.* Annals of Biomedical Engineering, 2009.

[3] M. Boulakia, J.-F. Gerbeau. *Parameter identification and POD reduced order modeling for cardiac electrophysiology.*

[4] Dale Dubin. *Lecture Accélérée de l'ECG*, 5e édition, Ed. Maloine, 2003.

[5] Laurent Dumas. Mémoire pour Habilitation à Diriger des Recherches. *Du transport de particules à l'optimisation globale sous contrainte d'équations aux dérivées partielles*, Université Pierre et Marie Curie - Laboratoire Jacques Louis Lions, 2008.

[6] John Fox. *Nonlinear Regression and Nonlinear Least Squares.* Appendix to An R and S-PLUS Companion to Applied Regression, 2002.

[7] Cordier Laurent, Bergmann Michel. *Proper Orthogonal Decomposition: an overview.* von Karman Institute for Fluid Dynamics, 2003.

[8] R. Fitzhugh. *Impulses and physiological states in theoretical models of nerve membrane. Biophys.* J., 1:445-465, 1961.

[9] Y. Goletsis, C. Papaloukas, D.I. Fotiadis, A. Likas, and L.K. Michalis. *Automated ischemic beat classication using genetic algorithms and multicriteria decision analysis.* IEEE Trans. Biomed. Eng., 51(10):17171725, 2004.

[10] J. Malmivuo, R. Plonsey. *Bioelectromagnetism. Principles and applications of bioelectric and biomagnetic fields.* Oxford University Press, New York, 1995.

[11] A. Illanes Manriquez, Q. Zhang, C. Medigue, Y. Papelier, M. Sorine. *Electrocardiogram-Based Restitution Curve.*

[12] Colleen C. Mitchell, David G. Schaeffer. *A two-current model for the dynamics of cardiac membrane.* Bulletin of Mathematical Biology 65, 767-793, 2003.

[13] J.S. Nagumo, S. Arimoto, and S. Yoshizawa. *An active pulse transmission line stimulating nerve axon.* Proc. IRE, 50:2061-2071, 1962.

[14] B. F. Nielsen, M. Lysaker, A. Tveito. *On the use of the resting potential and level set methods for identifying ischemic heart desease: An inverse problem.* Journal of Computational Physics 220, 772-790, 2007.

[15] M. Potse, R. Coronel, A.-R. LeBlanc, A. Vinet. *The role of extracellular potassium transport in computer models of the ischemic zone.* Med. Biol. Eng. Comput., 45(12):1187-1199, 2007.

[16] M. Potse, A. Vinet, J. G. Diodati, A.-R. LeBlanc, R. Nadeau. *Global subendocardial ischemia can explain ST depression in chronic angina.* Can. J. Cardiol., 23 Suppl. C:145C, 2007.

[17] M. Potse, A. Vinet, A.-R. LeBlanc, J. G. Diodati, R. Nadeau. *Understanding ST depression in the stress-test ECG.* Anatol. J. Cardiol., 7 Suppl. 1:145-147, 2007.

[18] M.Potse, R. Coronel, S. Falcao, A.-R. LeBlanc, A. Vinet. *The effect of lesion size and tissue remodeling on ST deviation in partial-thickness ischemia.* Heart Rhythm, 4(2):200-206, 2007.

[19] Z. Qu, Y. Xie, A. Garnkel, and J. N. Weiss. *T-wave alternans and arrhythmogenesis in cardiac diseases.* Frontiers in physiology, 1, 2010. art 154.

[20] J.M. Roger and A.D. McCulloch. *A collocation-Galerkin nite element model of cardiac action potential propagation.* IEEE Trans. Biomed. Engr., 41(8):743-757, 1994.

[21] Q. Zhang, A. Illanes Manriquez, C. Medigue, Y. Papelier, M. Sorine. *Robust and efficient location of T-wave ends in electrocardiogram.* Computers in Cardiology IEEE Computer Society 2005;32:711-714.

[22] Néjib Zenzemi. Mathematical doctoral thesis. *Étude théorique et numérique de l'activité élecrtique du coeur: Applications aux électrocardoigrammes,* INRIA - Université Paris-Sud 11, 2010.